

# Dimensional Design for Surface-Enhanced Raman Spectroscopy

Li Long,<sup>†</sup> Wenbo Ju,<sup>\*,†</sup> Hai-Yao Yang, and Zhiyuan Li<sup>\*</sup>Cite This: *ACS Mater. Au* 2022, 2, 552–575

Read Online

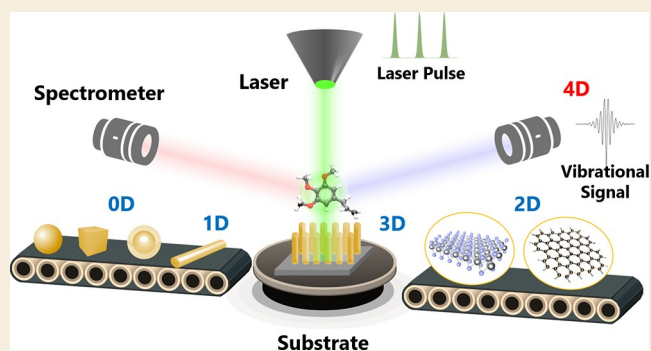
ACCESS |

Metrics &amp; More

Article Recommendations

**ABSTRACT:** Surface-enhanced Raman spectroscopy (SERS) is a vibrational spectroscopy technique that enables specific identification of target analytes with sensitivity down to the single-molecule level by harnessing metal nanoparticles and nanostructures. Excitation of localized surface plasmon resonance of a nanostructured surface and the associated huge local electric field enhancement lie at the heart of SERS, and things will become better if strong chemical enhancement is also available simultaneously. Thus, the precise control of surface characteristics of enhancing substrates plays a key role in broadening the scope of SERS for scientific purposes and developing SERS into a routine analytical tool. In this review, the development of SERS substrates is outlined with some milestones in the nearly half-century history of SERS. In particular, these substrates are classified into zero-dimensional, one-dimensional, two-dimensional, and three-dimensional substrates according to their geometric dimension. We show that, in each category of SERS substrates, design upon the geometric and composite configuration can be made to achieve an optimized enhancement factor for the Raman signal. We also show that the temporal dimension can be incorporated into SERS by applying femtosecond pulse laser technology, so that the SERS technique can be used not only to identify the chemical structure of molecules but also to uncover the ultrafast dynamics of molecular structural changes. By adopting SERS substrates with the power of four-dimensional spatiotemporal control and design, the ultimate goal of probing the single-molecule chemical structural changes in the femtosecond time scale, watching the chemical reactions in four dimensions, and visualizing the elementary reaction steps in chemistry might be realized in the near future.

**KEYWORDS:** SERS, dimensional design, enhancing substrates, nanoparticle, nanowire, 2D material, nanostructure array, spatiotemporal resolution



## 1. INTRODUCTION

Raman effect is named after C. V. Raman, who discovered “a new type of light scattering”, representing the effect of fluctuations of atoms or molecules from their normal state.<sup>1</sup> The incident photons interact with atoms or molecules, and they are absorbed and subsequently emitted via the assistance of virtual electron states. Most photons are elastically scattered (Rayleigh scattering), while a small fraction of the scattered photons gains or loses energy, leading to a shift of photon frequency (Raman scattering). Rayleigh and Raman scattering are schematically shown in Figure 1a. The differences in energy are determined by the energy of the different vibrational and rotational states of molecules (Figure 1b). Therefore, Raman scattering reflects the chemical composition and structure information on materials by measuring the Raman shift spectra, which represents a chemical fingerprint of the substance. Raman spectroscopy provides a nondestructive analytic method and has been widely applied in surface science,<sup>2,3</sup> life science,<sup>4,5</sup> environmental science,<sup>6,7</sup> and so on.

The breakthrough in laser technology provides an intense monochromatic light source for Raman spectroscopy; even so,

the Raman scattering is still very low in intensity. The Raman cross section of a single molecule is in the range of  $10^{-24}$  to  $10^{-30}$   $\text{cm}^2\cdot\text{sr}^{-1}$ ,<sup>8</sup> which is approximately  $10^6$ ,  $10^{10}$ , and  $10^{14}$  times smaller than those for infrared, Rayleigh, and fluorescence processes, respectively.<sup>9</sup> The low intensity greatly limited the application scope of Raman spectroscopy until the discovery of surface-enhanced Raman spectroscopy (SERS) in 1974.<sup>10</sup> The Raman intensity of pyridine molecules is significantly enhanced when the molecules are adsorbed on the surface of a roughened silver (Ag) electrode consisting of a large amount of Ag nanostructures. Both experiments<sup>11</sup> and theoretical work<sup>12</sup> have suggested that SERS could enable the increase of Raman intensity by  $\sim 10^6$ . The phenomenon has

Received: January 11, 2022

Revised: April 21, 2022

Accepted: April 21, 2022

Published: May 10, 2022



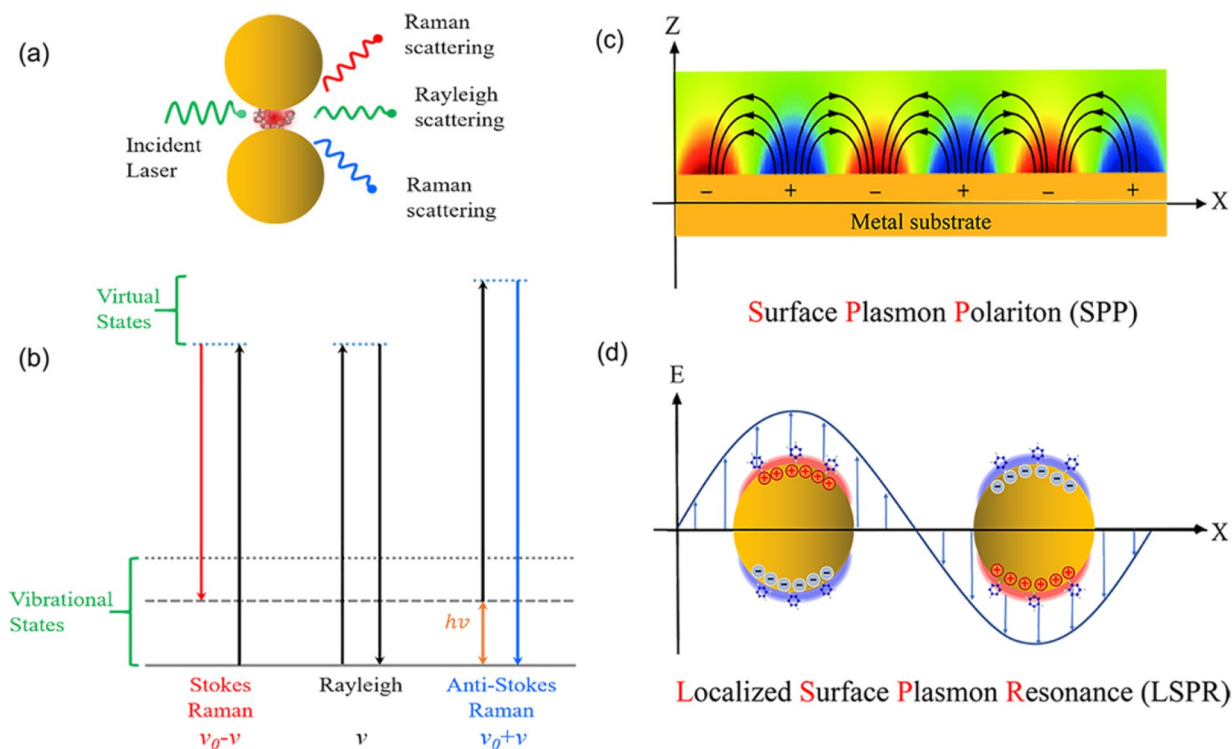


**Figure 1.** (a) Scheme of Raman and Rayleigh scattering of light by a molecule located between two metallic nanoparticles involving a hot spot. (b) Jablonski diagram representing the quantum energy transitions for Raman and Rayleigh scattering of a molecule. Schematic diagrams illustrating (c) surface plasmon polaritons at the surface of metal thin film and (d) localized surface plasmon resonance at metal nanoparticles.

been reasonably explained, and the concept of SERS has been proposed and has rapidly prospered since then.

SERS is considered to be a coincidence of several related effects produced generally by two mechanisms.<sup>13</sup> The electromagnetic mechanism (EM) is assigned to the surface plasmon resonances (SPRs), whereas the chemical mechanism (CM), which is still not well-understood, is attributed to the charge transfer resonances (CTRs). An early work shows that the overall enhancement factor (EF) of Raman radiation is up to a huge level of  $10^{15}$  in the platform of colloidal Ag nanoparticle aggregation, enabling the detection of single molecules,<sup>14</sup> although Le Ru et al.<sup>15</sup> demonstrated that SERS EFs as low as  $10^7$  are sufficient for the observation of single-molecule SERS signals. The nanogap between two adjacent Ag nanoparticles plays the key role in forming a prominent EM hot spot, where the EF of EM reaches a very high level (i.e.,  $10^{10}$ – $10^{12}$ ), many orders of magnitude larger than the EF of CM, which is at the modest level of 10–100. By contrast, a most recent work demonstrates that the EF of CM reaches  $\sim 10^6$  on the surface of porous carbon nanowires,<sup>16</sup> but unfortunately, the EF of EM is negligibly small. State-of-the-art plasmonic materials, which are coinage metals with nanoscale features, are widely used as substrates for SERS analysis, where EM plays the major role in the enhancement of Raman radiation.<sup>17,18</sup>

Performing a SERS experiment requires a careful choice of enhancing substrate due to the strong dependence of EFs on the interaction between analyte molecules and the nanostructured surface of substrates. SERS occurs preferentially at the interstices or sharp features of materials at micro/nanometer scales (Figure 2). In the early days of SERS, enhancing substrates are randomly roughened coinage metals fabricated by physical vapor deposition, electrochemical

roughening, or chemical etching.<sup>19</sup> Although the tunability of film thickness, morphology of metal islands, or separation of nanostructures has allowed variations of SERS signals to be detectable, a reliable platform for highly sensitive, stable, and reproducible outputs are still being sought, with emphasis on the quantitative optimization of SERS active sites.<sup>20–22</sup> The advances in nanoscience and nanofabrication have significantly reinvigorated the understanding and applications of SERS due to better-defined substrates at nanometer scales.<sup>23</sup> SERS substrates range in structures from zero-dimensional (0D) nanoparticles to one-dimensional (1D) nanowires or three-dimensional (3D) nanopillar arrays, with tunable SPRs, and range in compositions from coinage metals to nonmetallic two-dimensional (2D) materials (e.g., graphene and MXene), with tunable CTRs (Figure 2). The abilities to control the shape, orientation, arrangement of nanostructures, and surface compositions have reduced the inherent complexities of trace detection by SERS. The dimensionally well-defined nanostructures have paved the way for optimizing the amount of SERS active sites combined with the greatest EF for each site, establishing SERS as a robust and effective analytical technique for sensitive and selective detections of chemical substances.

This work reviews the dimensional design of enhancing substrates for SERS. It will not cover all publications in this field but will try to outline the development of SERS substrates in the nearly half-century history. In particular, we have categorized these SERS substrates into 0D, 1D, 2D, and 3D substrates according to their geometric dimension. We will show that, in each category of SERS substrates, design upon the geometric and composite configuration can be made to achieve an optimized EF of the Raman signal. We also show that the temporal dimension can be incorporated into SERS by applying femtosecond pulse laser technology, so that the SERS

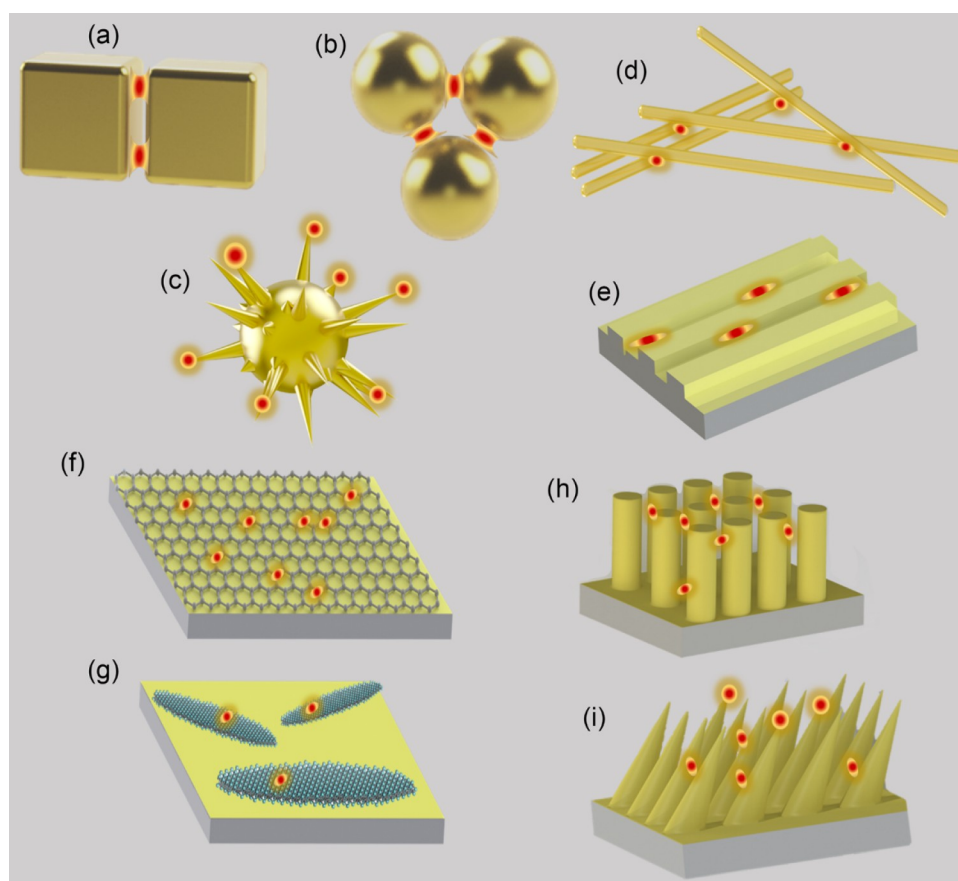


**Figure 2.** Schemes of several typical SERS substrates: one-dimensional (a) nanocube dimer, (b) nanoparticle trimer, and (c) spiked nanosphere; one-dimensional (d) nanowires and (e) nanogaps; two-dimensional (f) graphene and (g) MXene; Three-dimensional (h) nanopillar array and (i) nanocone array.

can be used not only to identify the chemical structure of molecules but also to uncover the ultrafast dynamics of the structural change of molecules. We will discuss this so-called four-dimensional (4D) SERS technology and the perspective for probing the structural changes of a single molecule in the femtosecond time scale, watching the chemical reactions in four dimensions, and visualizing the elementary reaction steps in chemistry. We expect that the improvement of SERS in the spatiotemporal resolution will significantly advance the understanding of some fundamental questions and extend SERS as a versatile technique for ultrafast analytical applications.

In section 2, we introduce briefly the fundamentals of SERS. In sections 3–6, SERS substrates ranging in structures from 0D to 3D are discussed. In section 7, we summarize the progress of Raman spectroscopy with high spatial and temporal resolution and suggest the 4D design for SERS in time and space domains. In the last part, we summarize the dimensional design for SERS and give a perspective on the roadmap of approaching the ultimate goal for SERS.

## 2. PRINCIPLE OF PLASMON-ENHANCED RAMAN SCATTERING

Theoretical, numerical, and experimental efforts on finding the light–matter interaction enhancement have indicated that SERS enhancement relies strongly on the optical resonance properties of nanostructures preferably made from coinage metal, such as Ag and gold (Au).<sup>24</sup> There are mainly two classes of excitation, which are identified as surface plasmon

polaritons (SPPs) at a metal–dielectric interface (Figure 1c) and localized surface plasmon resonance (LSPR) on the surface of metal nanoparticles (Figure 1d). SPR provides significantly enhanced optical electric fields in the vicinity of metallic nanostructures and increases the absorption and emission cross sections of analyte molecules. Figure 2 shows several typical geometric configurations of well-designed metallic nanostructures consisting of nanogaps. The nanogap is also known as a hot spot, which is capable of enhancing the incident light to a highly intense local electric field via LSPR and near-field scattering processes. In addition, a hot spot enhances the Raman radiation from the near-field to the far-field via some physical processes, such as resonance scattering or an optical antenna effect. The EF of Raman radiation, which is derived from the classical Raman scattering model, is given by<sup>24</sup>

$$g(r_0) = \frac{I(\omega_R)}{I_{\text{vac}}(\omega_R)} = \frac{|g(r_\infty, r_0, \omega_R)|^2}{|g_0(r_\infty, r_0, \omega_R)|^2} \times \frac{|E(r_0, \omega)|^2}{|E_0(r_0, \omega)|^2} \quad (1)$$

where  $g(r_\infty, r_0, \omega_R)$  is the total Green function, consisting of the free space Green function  $g_0(r_\infty, r_0, \omega_R)$ , and the scattering Green function  $g_S(r_\infty, r_0, \omega_R)$

$$g(r_\infty, r_0, \omega_R) = g_0(r_\infty, r_0, \omega_R) + g_S(r_\infty, r_0, \omega_R) \quad (2)$$

The Green functions describe basically the efficiency of radiation of a dipole. In principle, they are second rank tensors but are treated as scalars for simplicity

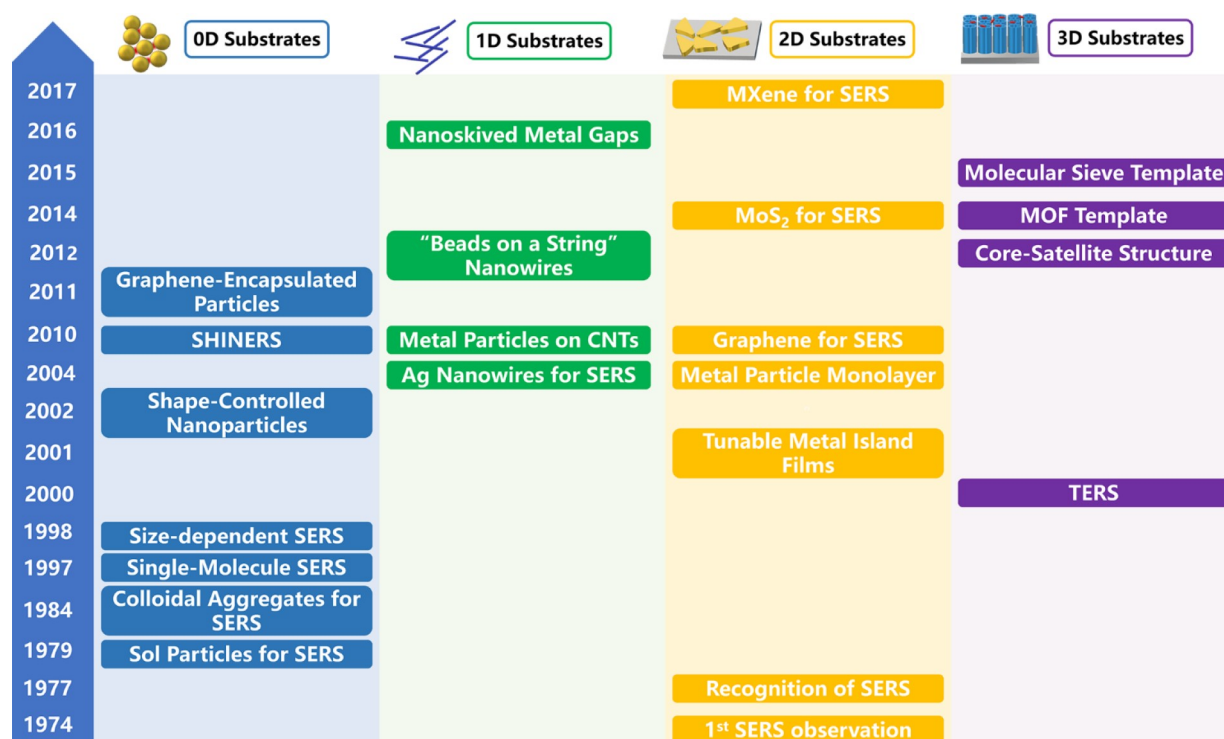


**Figure 3.** Some milestones in the development of SERS substrates made in the past nearly half-century history of SERS, including 0D nanoparticles, 1D nanowires, 2D metallic and nonmetallic thin films, and 3D nanostructure arrays. The advances of SERS substrates have significantly broadened the application scope of SERS.

$$g(r_0) = g_E(\omega) \times g_R(\omega_R) \quad (3)$$

where  $g_E(\omega)$  and  $g_R(\omega_R)$  are the EFs in the Raman excitation and radiation processes, respectively, for a molecule located at the site  $r_0$ .  $\omega$  is the angular frequency of incident light, and  $\omega_R$  is the Stokes, or anti-Stokes, frequency of Raman radiation. In fact, the excitation and radiation enhancement are closely related and are almost equal to each other. The difference between  $\omega_R$  and  $\omega$  is relatively small. As a result, we can simplify the eq 1 to get

$$g(r_0) = \frac{|E(r_\infty, \omega_R)|^2}{|E_0(r_\infty, \omega_R)|^2} \times \frac{|E(r_0, \omega)|^2}{|E_0(r_0, \omega)|^2} = \frac{|E(r_0, \omega)|^4}{|E_0(r_0, \omega)|^4} \quad (4)$$

The EF of Raman radiation is approximately equal to the fourth power of the local electric field enhancement ratio.

On the basis of the classical model, Zhang et al.<sup>25</sup> established a new Raman scattering theory, in which the collective and cooperative actions of Rayleigh and Raman scattering of molecules are taken into account. When a molecule locates near a hot spot, the EF follows the equation

$$g(r_0) = \frac{|E(r_0, \omega)|^4}{|E_0(r_0, \omega)|^4} \cdot g^4(r_0, \omega) \quad (5)$$

where  $g^4(r_0, \omega)$  is an amendment factor. This amendment factor involves the contributions of Rayleigh scattering by molecules and the self-interaction caused by the multiple scattering by nanostructures and molecules. For the tip-enhanced Raman spectroscopy (TERS) system, the amendment factor is also available. The movement of a molecule at a hot spot generates a simultaneous change of the local electric field, leading to the change of Raman signal. The new Raman

scattering theory can explain the ultrahigh spatial resolution (about 1 nm) of TERS. Hitherto, the complete principles of Raman enhancement have not yet been established, requiring further investigations to cover all qualitative and quantitative details.

Since the enormous enhancement of the spectroscopic signature of a single molecule was demonstrated on the surface of aggregated Au nanoparticles,<sup>14</sup> the detection limit of SERS has been pushed downward to the single-molecule level. In experiments, there are still two major problems with SERS. One is that analyte molecules can only obtain a strong Raman scattering when they are absorbed on the surface of coinage metals and some alkali metals. Other metals have not yet been identified as active substrates for SERS. The other problem is that only roughened metal surfaces are active for SERS. The size and morphology, in addition to the surface composition, of nanostructures play significant roles in the EF of Raman radiation. Thus, many efforts have been made to synthesize SERS active nanostructures with controlled size, shape, and curvature. The regions with a high curvature exhibit the well-known "lightning rod effect", where a strong SERS signal can be achieved via the electric field enhancement. Anisotropic nanoparticles, such as nanocages,<sup>26</sup> nanocubes,<sup>27</sup> and nanopolyhedron,<sup>28</sup> are demonstrated as highly active SERS substrates. The modification of nanostructure morphology via postsynthesis, rather than the direct synthesis of complex nanoparticles, has been investigated for SERS substrates with a high density of hot spots.<sup>29,30</sup> Additionally, multidimensional SERS substrates have been extensively developed in order to obtain regular nanogaps for desired plasmonic coupling and local electric field enhancement. Self-assembled nanoparticle arrays, especially at liquid/liquid or liquid/air interfaces, have interstices with tunable density and width, which are suggested

as robust and reproducible platforms for the detection of multianalytes.<sup>31</sup>

In addition to the geometric design of SERS substrates, it is interesting to further incorporate some time-resolved techniques into the ordinary SERS, leading to the development of the so-called spatiotemporal SERS technology, where ultrafast pulse laser technology with an adjustable wavelength works collectively with the surface plasmon enhancement of weak Raman optical signal technology.<sup>32–36</sup> Femtosecond time-resolved Raman spectroscopy has become an effective method to obtain high-resolution vibrational spectra with molecular vibrational lifetimes on the order of nanoseconds or picoseconds. This method provides an amazingly powerful route for probing the chemical structure and dynamic state of molecular vibration and rotation at the level of atomic motion. This relatively new Raman spectroscopy has been effectively used to study the intermolecular vibration of liquids,<sup>37,38</sup> collective and alienating movement in proteins,<sup>39,40</sup> and solid phonon modes.<sup>41</sup>

Figure 3 summarizes a timeline of some important developments of SERS techniques from the aspect of dimensional design in the past half century. SERS substrates can be made from 0D nanoparticles, 1D nanowires, 2D metallic thin films, nonmetallic 2D materials, or 3D nanostructure arrays. A large number of studies have focused on the regulation of composition and morphology, the concentration of hot spots, and surface chemical modification to improve the performance of SERS substrates. The sensitivity of SERS has been increased for the detection of a single molecule. On the other hand, researchers focus on Raman imaging via the technology of TERS and continually push down the spatial resolution to the nanometer level.<sup>25,42–46</sup> Another frontier of Raman spectroscopy is actively explored by incorporating ultrafast pulse lasers to excite and probe the structural changes of a molecule with a temporal resolution down to nanosecond, picosecond, and femtosecond time scales. These topics and technologies will be briefly introduced and discussed in the following sections, with a hope to harness and evaluate rich experiences and lessons made and accumulated in the past and find a pathway to push up the ultimate limit of Raman spectroscopy to an unprecedented level in terms of intensity, spatial, temporal, or spectral resolution, either separately or collectively.

### 3. SERS SUBSTRATE MADE FROM 0D METAL NANOPARTICLES

The 0D SERS substrates discussed in this work refer particularly to the functional nanoparticles or nanocrystals with a size less than 100 nm in all three dimensions. Since the first report of Au and Ag sol particles as SERS substrates in 1979 by Creighton et al.,<sup>47</sup> nanoparticles made from coinage metals or their alloys have been intensively investigated for SERS, which have high sensitivity and reliability. In the early stages of 0D SERS substrates, sol particles prepared by a wet chemical synthesis are supposed to be roughly spherical with a large size distribution.<sup>47</sup> The particle size is estimated using the Mie's extinction data of metal sols, and it is determined that the primary and aggregated Au particles have a radii of <30 and  $\geq 90$  nm, respectively. The first well-defined 0D SERS substrates are described by Natan and co-workers.<sup>48</sup> The self-assembly of monodisperse Au and Ag colloid particles has tunable particle size and interparticle spacing, making the control of EF available.<sup>49</sup> The sophisticated control of particle

size and shape, interparticle spacing, or even the surface composition of 0D SERS substrates has greatly enhanced both the fundamental understanding and practical applications of SERS.

The isolated spherical particle model is the simplest one for the SPR simulation, and its EF has been theoretically calculated.<sup>12,50</sup> The theoretical study of EFs for small metal particles by Schatz and co-workers predicts that the excitation wavelength associated with the peak field enhancement depends on the particle size, and the relationship is roughly linear for large-size particles.<sup>51</sup> Nie and co-workers used spatially isolated Ag colloidal nanoparticles with a narrow size distribution for SERS and successfully observed an approximately linear relationship, agreeing well with the theoretical calculations.<sup>52</sup> For isolated spherical Au nanoparticles, the maximum excitation wavelength and EF depend on the particle size, and interestingly, the maximum EF is obtained with Au nanoparticles in the size range from 60 to 70 nm.<sup>53,54</sup> The model of SPR at an isolated spherical particle is successful to some extent, including the prediction of the size-dependent property for SERS, but the calculated EF from this model is smaller than  $10^3$ , which hardly agrees with most experimental SERS data.<sup>55</sup> Thus, the numerical analysis of SERS from an isolated particle model is quantitatively not sufficient. Many studies suggest that the electromagnetic coupling of neighboring particles should be taken into account for the  $10^3$ – $10^4$  extra EFs.<sup>56,57</sup>

The morphology control of nanoparticles via solution-based chemical processes has paved the way for the investigation of shape-dependent EFs. The morphologies of nanoparticles can be controlled by adjusting the temperature, pH, or reactant concentration, by adding complementary surfactants, or by exposing nanoparticles to various external stimuli including light, heat, and magnetic field.<sup>58,59</sup> Nanoparticles with various well-defined morphologies, such as nanorods,<sup>60,61</sup> nanocubes,<sup>62,63</sup> nanoprisms,<sup>64,65</sup> nanospheres,<sup>66,67</sup> and nanostars,<sup>68,69</sup> have been successfully synthesized via solution routes. Since monometallic nanoparticles with a sharp edge or angle can intensify the electric field in the vicinity of the high curvature regions, an extra SERS enhancement is theoretically derived and assumed to be due to the "lightning rod effect",<sup>70</sup> and this effect is experimentally observed on coinage metal nanorods and nanocubes.<sup>71–73</sup> Kedia and Kumar<sup>68</sup> adjusted the basicity of synthetic precursors to reshape the morphology of Au nanoparticles from hyperbranched nanostars to nanospheroids. In transition, the two strong LSPR peaks for the Au nanostars merge into a broad singular one, successfully correlating the SERS signal to the nanostructures of substrates.

Since the prominent high-yield synthesis of Ag nanocubes was innovated by Sun and Xia,<sup>74</sup> the properties of single-crystal metallic nanocubes have been intensively investigated due to their structural specificities including atomically flat facets and orthogonal facets and edges. As a model substrate, nanocubes facilitate the understanding of structure- or geometry-dependent EFs. For an individual nanocube, a larger EF is recorded when the nanocube is oriented with a face diagonal axis rather than its edge, parallel to the illuminating laser polarization.<sup>75</sup> Ag nanocube dimers with different geometric configurations enable the adjustment of hot spots located at the junctions between two or more closely adjacent Ag particles.<sup>75,76</sup> The EF on the order of  $10^7$  is achieved from the dimers displaying a face-to-face or edge-to-face configuration, which is 1 order of

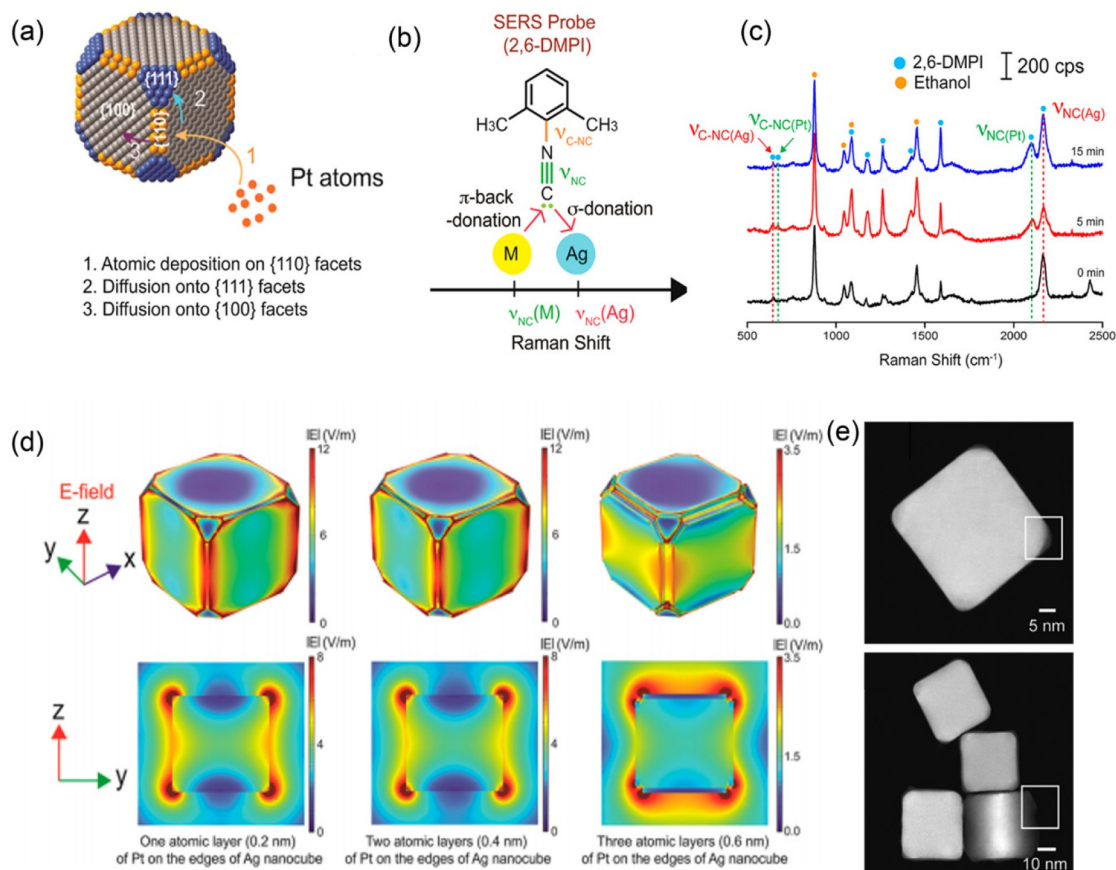


**Figure 4.** Schematic illustration of (a) a Ag nanocube decorated selectively by Pt atoms and (b) the difference in stretching frequency for the N≡C bond when the isocyanide group binds to Ag or M atoms. (c) Time-dependent SERS spectra of 2,6-dimethylphenyl isocyanide recorded from an aqueous mixture of 39 nm Ag nanocubes, ascorbic acid, and poly(vinylpyrrolidone) after the addition of a  $\text{H}_2\text{PtCl}_6$  solution. (d) Calculated electric field distributions on a 39 nm Ag nanocube with different numbers of Pt atoms deposited on the edges and {110} facets of the nanocube. (e) High-angle annular dark-field scanning TEM images of a sample obtained by reacting the 39 nm Ag nanocubes. Adapted from ref 80. Copyright 2017 American Chemical Society.

magnitude higher than that from dimers with an edge-to-edge configuration. Hence, the relative orientation of nanocubes, which correlates to the number of probe molecules enclosed in the hot spot region, is a key factor for EF.<sup>75</sup>

Bimetallic nanoparticles are of interest to SERS applications due to the additional tunability as compared to their monometallic counterparts. The configurations of bimetallic nanoparticles are commonly bulk and surface alloys and core-shell structures. The alloyed nanoparticles consist of both metal atoms on the surface, so that the SERS enhancement depends on the initial composition of the alloyed nanoparticles,<sup>77,78</sup> as well as on the evolution of the elemental ratio on the surface.<sup>79</sup> Zhang et al. deposited Pt atoms selectively at the edges of Ag nanocubes and then at the corners and on the facets via diffusion (Figure 4a). Isocyanide-based molecules function as ultrasensitive probes for the in situ characterization of the growth of Pt on Ag nanocubes, as the N–C stretching frequency for adsorbed isocyanide groups on Ag is different than that on Pt (Figure 4b). The SERS of molecular probes on bimetallic nanoparticles is capable of elucidating the mechanistic details involved in the seeded overgrowth of a catalytically significant metal, such as Pt, Pd, Ir, Rh, and Ru, on the surface of Ag or Au nanocrystal seeds (Figure 4c–e).<sup>80</sup> The core-shell bimetallic nanoparticles, on the other hand, represent a structure in which one metal termed as the core is completely surrounded by another metal termed as the shell.

Tian and co-workers<sup>81</sup> deposited several atomic layers of a Pt group metal on a highly SERS active Au nanoparticle and utilized the core-shell bimetallic nanoparticles to detect the SERS of adsorbed water on Pt or Pd. The core-shell nanoparticles have the chemical properties of the shell but show a high electromagnetic enhancement of the Au core. This strategy has advanced the study of Raman radiation of some molecules (e.g., water) with a low Raman cross section, which were practically impossible in the past.

A metallic nanoparticle core with a nonmetallic shell forms another type of 0D SERS substrates with a core-shell configuration. The relevant technique develops into a big branch of SERS, which is called shell-isolated nanoparticle-enhanced Raman spectroscopy (SHINERS).<sup>82</sup> The plasmonic nanoparticles for SHINERS are completely covered by a shell of nonplasmonic materials. The chemically inert shell protects the plasmonic core from contamination or aggregation but does not significantly damp the surface electromagnetic enhancement.<sup>83</sup> Tian and co-workers<sup>82</sup> demonstrated the first SHINERS experiment using Au nanoparticles coated with an ultrathin silica or alumina shell (Figure 5a,b). The core-shell nanoparticles are directly deposited onto the surface under study and induce a large local electric field enhancement. Nanoparticles for SHINERS avoid the direct contact of the plasmonic nanoparticles with the analyte surface, which is very important for analyzing biological samples, as

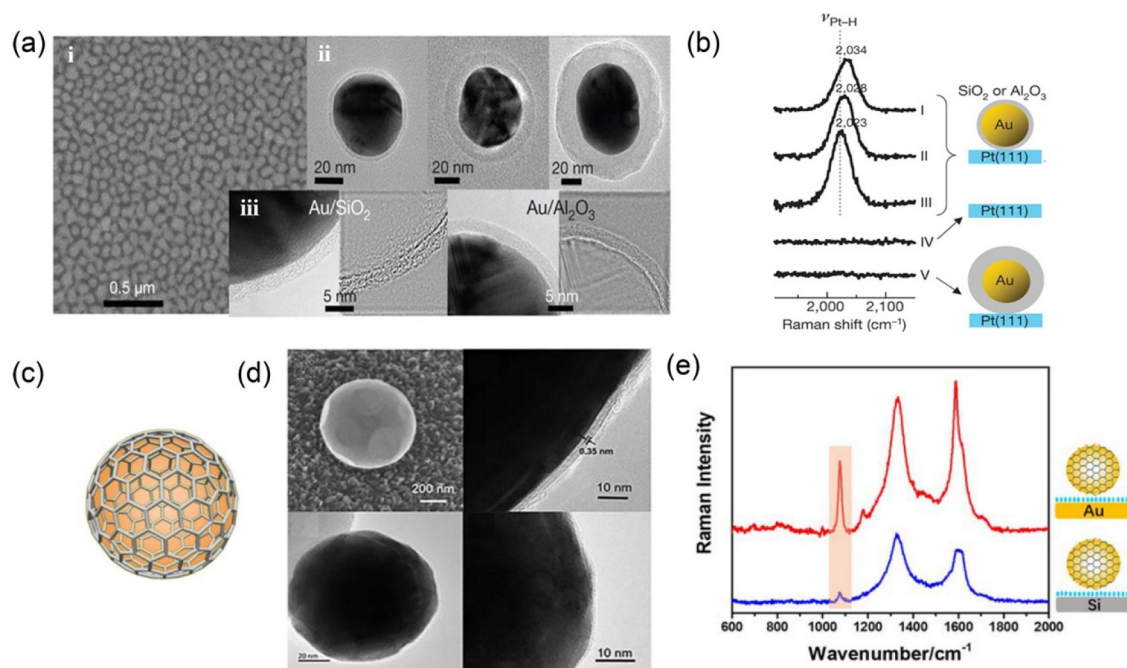


**Figure 5.** (a) SEM and high-resolution TEM images of Au@SiO<sub>2</sub> and Au@Al<sub>2</sub>O<sub>3</sub> shell-isolated nanoparticles with different shell thicknesses. (b) Potential dependent SHINERS spectra for hydrogen adsorbed on a Pt(111) surface captured with/without shell-isolated nanoparticles. (c) Scheme of a graphene-coated Au nanocrystal (Au@G). (d) SEM and high-resolution TEM images of Au@G. (e) SERS spectra of Au@G nanoparticles assembled on a Au substrate and a silicon substrate with mercaptobenzoic acid. Panels (a,b) were adapted with permission from ref 82. Copyright 2010 Springer Nature. Panels (c–e) were adapted with permission from ref 93. Copyright 2021 John Wiley & Sons, Ltd.

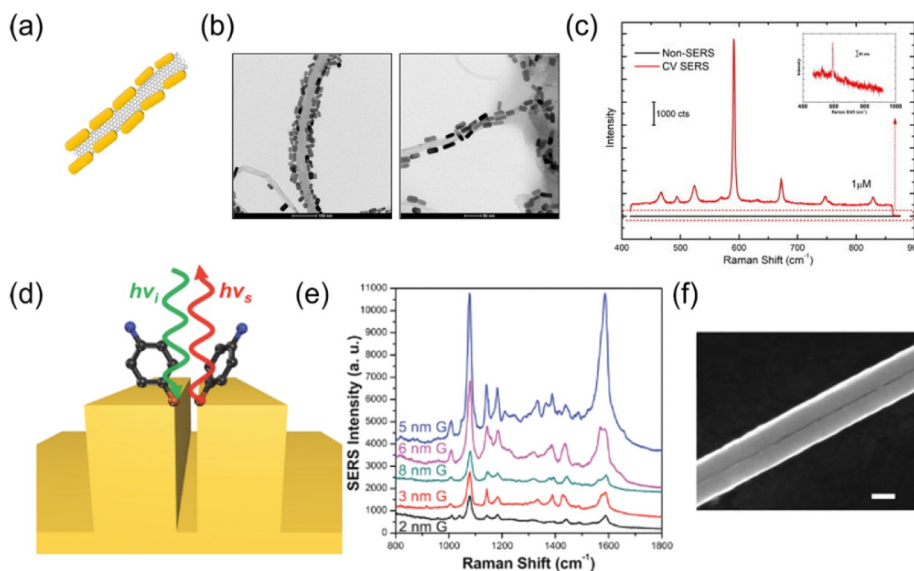


**Figure 6.** (a) Scheme of a CNT/Au nanorod hybrid. (b) TEM images of multiwalled carbon nanotube (MWCNT)/Au nanorod hybrids. (c) SERS spectra of 1  $\mu$ M cresyl violet obtained from the coffee ring formed by the MWCNT/Au nanorods hybrids and without enhancement (inset). (d) Illustration of the SERS workbench principle for the standing nanogap. (e) Experimentally recorded dependence of the SERS intensity versus gap width from 2 to 8 nm. (f) SEM image of a 1D Au nanogap with the gap width of 3 nm. Panels (a–c) were adapted with permission from ref 102. Copyright 2015 Elsevier Inc. Panels (d–f) were adapted with permission from ref 106. Copyright 2016 Wiley-VCH Verlag GmbH & Co. KGaA, Weinheim.

some plasmonic nanoparticles have potential risks to change the structure of biomolecules via interactions. In addition to Au cores, Ag and Au@Ag<sup>84–86</sup> plasmonic cores are used for SHINERS, and in some cases, the Ag-based cores are more efficient for SERS enhancement. The ultrathin protective shells are generally oxides with high chemical resistance, such as silica, titania, or zirconia,<sup>83</sup> but they are not limited to these

materials. Some other materials, such as gelatin,<sup>87</sup> carbon,<sup>88–91</sup> and organic polymers,<sup>92</sup> are used for the same purpose. A very recent work from Tian's group<sup>93</sup> demonstrates the graphene-coated Au nanoparticles for SHINERS (Figure 5c). The thickness of the graphene shell can be precisely controlled in the chemical vapor deposition (Figure 5d,e). The graphene-coated Au nanoparticles have extremely high stabilities in

solutions with pH values from 1 to 13 and at temperatures from ambient up to 300 °C.

#### 4. SERS SUBSTRATE MADE FROM 1D NANOWIRES

One-dimensional SERS substrates represent materials with the size in two dimensions less than 100 nm and much larger in the third dimension, such as nanowires, nanorods, nanobelts, and nanotubes. The development of 1D SERS substrates is driven by the controlled and reproducible formation of interstitial spaces between metallic nanostructures, as hot spots, which are present within the interstitial spaces, have been claimed to provide extraordinary SERS enhancements of around 14 orders of magnitude.<sup>14,94</sup> Several 1D model structures, including single nanowires,<sup>95</sup> nanoparticle–nanowire junctions,<sup>96</sup> nanowire dimers,<sup>97</sup> and nanowire bundles,<sup>98</sup> are used for SERS. Moskovits and co-workers<sup>99</sup> fabricated flat arrays of aligned Ag nanowires by electrodepositing Ag in the nanopores of highly ordered anodic aluminum oxide (AAO) templates and measured the SERS signal from Rhodamine 6G (R6G) molecules adsorbed onto the completely released Ag nanowires. The giant SERS effect with single-molecule detection is obtained within the gaps between two parallel nanowires when the polarization of the optical electric field is perpendicular to the longitudinal axis of nanowires. They also develop a partial etching process, allowing the exposure of the topmost Ag nanowires from AAO templates. Analyte molecules are adsorbed within the nanogaps created by collapsing nanowire tips, and the detection sensitivity benefits from the high electric field existing in those hot spots.<sup>98</sup> This strategy creates hot spots in the interstices between adjacent nanowire dimers, which is in effect comparable to the scheme of nanoparticle dimers. Its counterpart is to generate dense hot spots on a single 1D substrate. Gunawidjaja et al.<sup>100</sup> decorated Ag nanowires with Au nanoparticles to form a bimetallic hierarchical structure. Chen et al.<sup>101</sup> modified the surface of Ag nanowires with Ag nanoparticles. Goh et al.<sup>30</sup> generated “beads on a string” features of 1D Ag nanowires using anisotropic chemical etching. These methods overcome the limitations of SERS hot spots located at the tips or in the interstices of 1D Ag nanowire arrays and increased the SERS hot spots across the longitudinal axis of nanowires. Meanwhile, the polarization-independent SERS signals are significantly enhanced. The size and spacing of plasmonic nanostructures deposited on the nanowires provide additional parameters to tune the maximum excitation wavelength and EF. Carbon nanotubes (CNTs) are the most representative 1D materials with a large specific surface area. The decoration of CNTs with plasmonic nanoparticles forms 1D SERS substrates with a high density of hot spots.<sup>102–104</sup> The composites of Ag or Au nanoparticles and CNTs have reported detection limits from  $10^{-9}$  to  $10^{-12}$  mol·L<sup>-1</sup> (Figure 6a–c).<sup>102</sup>

It is possible to fabricate 1D SERS substrates directly on a solid substrate via a top-down approach using lithography or template techniques.<sup>105</sup> Zhou et al.<sup>106</sup> demonstrated a scalable nanofabrication approach based on nanoskiving to create a series of 1D millimeter-long nanogaps with tunable sub-10 nm gap widths (Figure 6d–f). These model structures have successfully linked the simulated electric field distributions in nanogaps and experimentally recorded SERS signals. The nanogap with a gap width of 5 nm is optimum for obtaining the strongest plasmonic coupling, and its EF is 250 times greater than that of an individual Au nanowire. The nanoskiving technique can be extended to fabricate 2D

nanogap arrays and 3D nanogap grids, providing a series of SERS substrates for systematic investigation of the dependence of SERS enhancements on the gap widths, crossing points, and electric field polarizations.

#### 5. SERS SUBSTRATES MADE FROM ULTRATHIN METALLIC STRUCTURES AND 2D MATERIALS

Two-dimensional SERS substrates have one dimension in the nanometer scale, including metallic thin films, ultrathin metallic structures, and emerging 2D materials, such as graphene, hexagonal boron nitride (h-BN), transition metal dichalcogenides (TMD), MXene, and black phosphorus.

##### 5.1. Ultrathin Metallic Structures

Flat coinage metal thin films are not typical SERS active substrates, but the ones containing nanogaps demonstrate highly intense hot spots. Weimer and co-workers<sup>20,107</sup> deposited Ag and Au islands on glass substrates under precise control, and they were able to adjust the SERS wavelengths throughout the visible and even into the near-infrared regions of the spectrum. Au@SiO<sub>2</sub> core–shell nanoparticles for SHINERS<sup>82</sup> are spread over the probed surface to form a monolayer, conforming to different contours of substrates. The fabrication of a large-area 2D metallic nanoparticle monolayer is achieved through the oil–water interfacial self-assembly of charged colloidal nanoparticles, which provides large void areas and nanogaps without the assistance of molecular ligands.<sup>108</sup> Au nanoparticle monolayers with sub-1 nm gaps are fabricated for SERS with maximum EFs on the order of  $10^{11}$ , and their stretchable version supported on a poly(dimethylsiloxane) substrate retains similar SERS intensities in the state of stretching or relaxation. Lin et al.<sup>109</sup> constructed layer-by-layer assemblies of Ag nanocubes and observed a gradually enhanced SERS intensity with the increase of the number of layers from 1 to 4.

Nanosphere lithography (NSL) is an inexpensive, inherently parallel, high-throughput nanofabrication technique capable of producing a large variety of nanoparticles and well-ordered 2D nanoparticle arrays with height in the range of several tens of nanometers. The process involves drop-coating a polymer nanosphere to self-assemble into a close-packed hexagonal array and then using this array as a mask for the deposition of various metallic nanostructures.<sup>110</sup> A multitude of nanostructural motifs, including nanoparticles, nanotriangles, nanorings, nanogaps, and nanoparticle chains, have been constructed using NSL.<sup>110–113</sup> These model structures have advanced the understanding of the dependence of LSPR on material, size, shape, interparticle spacing, and other important factors. Some conclusions are still considered as the “golden rules” for the design of SERS substrates.

Electron beam lithography (EBL) is used to fabricate ultrathin metallic structures supported on flat substrates, which is proposed to be superior to SERS applications.<sup>114</sup> The metallic structures shaped by EBL are mainly periodic arrays of some patterns. Kahl et al.<sup>115</sup> introduce EBL as a new method to achieve a regularly structured SERS surface formed of Ag nanoparticles. Two different methods have been presented in this framework, the lift-off approach and the etching method. In the lift-off process, a Ag layer is evaporated on the structured resist, and the resist is removed afterward, leaving regular fields of Ag nanoparticles. The etching method, in contrast, constructs Ag gratings or crossed gratings onto a silicon wafer by reactive ion etching and Ag evaporation.

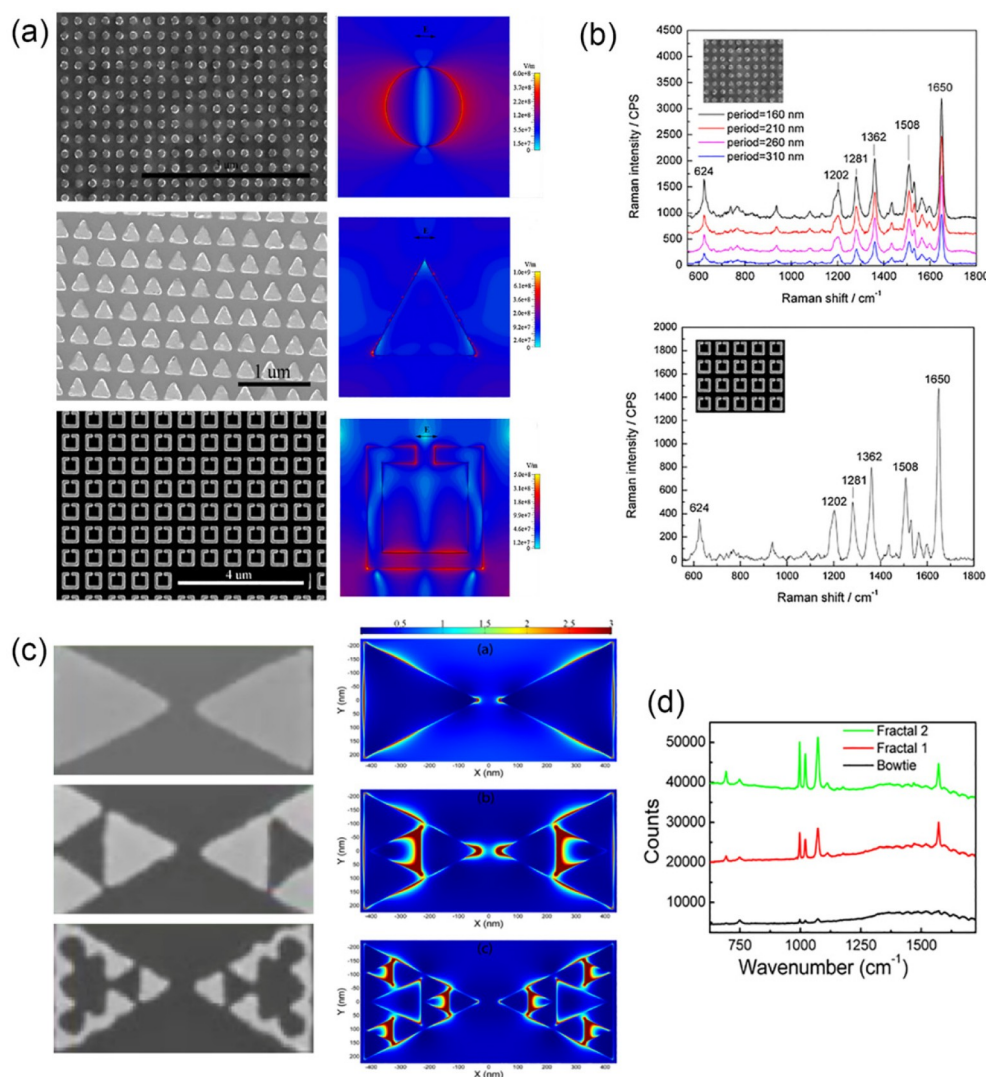


**Figure 7.** (a) SEM images of Au nanodiscs (top), triangular dots (middle), and split rings (bottom) and their corresponding electric field distributions simulated at the frequency equivalent to the Raman excitation wavelength of 532 nm. (b) SERS spectra of R6G on the array of Au nanodisc array with the period of 160–300 nm (top) and the spectrum of R6G on the array of Au split rings. (c) SEM images of bowtie (top), Fractal-1 (middle), and Fractal-2 (bottom) structures and their corresponding electric field distributions at the Stokes shifted wavelength of 895 nm. (d) SERS measurement results for the three structures. Panels (a,b) were adapted with permission from ref 117. Copyright 2012 IOP Publishing Ltd. Panels (c,d) were adapted with permission from ref 120. Copyright 2014 The Optical Society.

Beermann et al.<sup>116</sup> constructed rectangular 50 nm high nanoparticles of different sizes on the surface of a smooth Au film and arranged them both individually (i.e., placed sufficiently far apart) and in 740 nm period arrays. Linear reflection spectra and high-resolution Raman images obtained from arrays of nanoparticles are compared, revealing good correspondence in the spectral dependences of reflection and local SERS enhancements. Yue et al.<sup>117</sup> fabricated nanostructured Au substrates with precisely controlled geometries and arrangements. The geometries of nanostructures fabricated by the lift-off process include nanogratings (60 nm line width), nanodiscs (110 nm diameter), triangular dots (100 nm edge length), and split rings (160 nm cell size and 20 nm arm width). The geometries of nanostructures fabricated with EBL combined with plasma etching include rhombus nanoholes (100 nm edge length), circular nanoholes (200 nm diameter), nanogrids, and split rings (Figure 7a). The enhancement of the Raman signal depends significantly on the geometry and arrangement of Au nanostructures (Figure 7b). The EFs on

nanogratings are almost 1 order of magnitude higher than those on other nanostructures. In addition, the SERS enhancement on the nanostructures fabricated with the lift-off process is higher than that on the same nanostructures fabricated with the plasma etching. EBL is also used to fabricate more complex patterns, such as coupled Au rings,<sup>118</sup> bowties,<sup>119</sup> and fractal bowties.<sup>120</sup> The fractal plasmonic structures are advantageous to a controlled broadband spectral response.<sup>121</sup> The experimental work and numerical simulation done by Cakmakyapan et al.<sup>120</sup> show that the response of the fractal bowtie antennas goes to longer wavelengths after each fractalization step, and the fractal geometry provides multiple hot spots on the surface, which can be used efficiently for SERS (Figure 7c,d).

## 5.2. 2D Materials

The active innovations in 2D materials in the last two decades have significantly expanded and extended the family of SERS substrates. Graphene is commonly recognized as the first

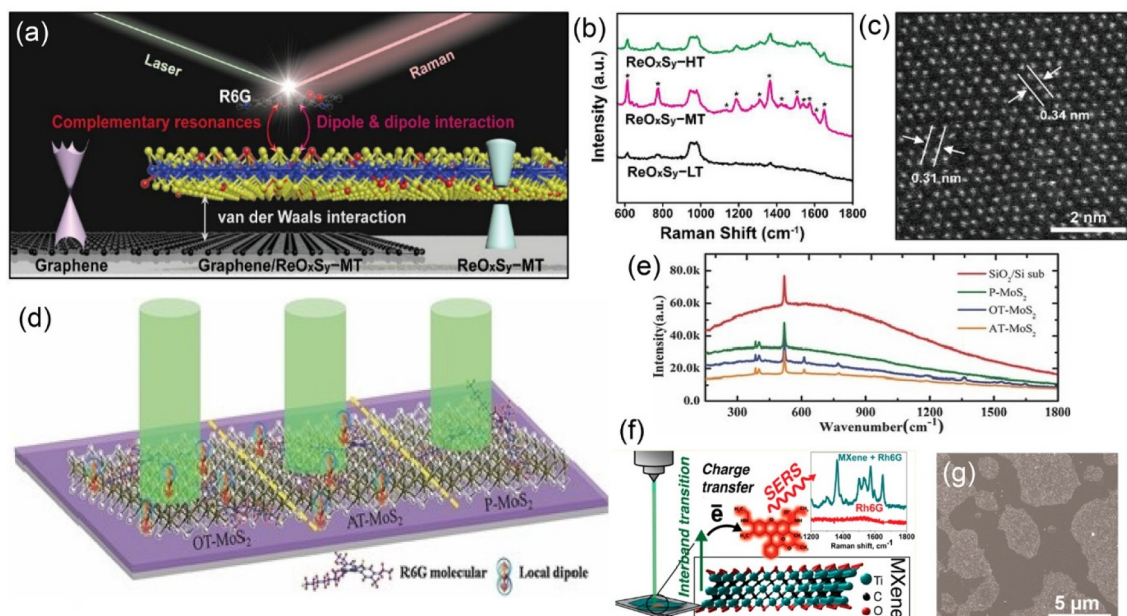


**Figure 8.** (a) Schematic illustration of SERS for R6G molecules on the graphene/ReO<sub>x</sub>S<sub>y</sub>-MT vertical heterostructure. (b) SERS spectra of R6G (10<sup>-4</sup> M) on the ReO<sub>x</sub>S<sub>y</sub> film prepared at different sulfurization temperatures. (c) Atomic resolution scanning TEM image of ReO<sub>x</sub>S<sub>y</sub>-HT. Schematic illustration (d) and Raman spectra (e) of R6G molecules on various MoS<sub>2</sub> substrates. (f) Schematic illustration of a Ti<sub>3</sub>C<sub>2</sub>T<sub>x</sub> SERS substrate and (g) SEM image of Ti<sub>3</sub>C<sub>2</sub>T<sub>x</sub> supported on glass. Panels (a–c) were adapted from ref 126. Copyright 2020 American Chemical Society. Panels (d,e) were adapted with permission from ref 128. Copyright 2014 Wiley-VCH Verlag GmbH & Co. KGaA, Weinheim. Panels (f,g) were adapted from ref 135. Copyright 2017 American Chemical Society.

“modern” 2D material, with a thickness of a single or a few atomic layers.<sup>122</sup> The SERS of probe molecules on the surface of graphene is first reported by Ling et al.<sup>123</sup> The EF depends strongly on the distance between chemical groups and graphene<sup>124</sup> and the number of graphene layers,<sup>125</sup> indicating the importance of a CM for Raman enhancement. The combination of graphene and metallic heterogeneous nanostructures is an effective strategy to improve the SERS activity of graphene and, in some cases, can be harnessed to overcome the disadvantages of heterogeneous SERS substrates. After the discovery of SERS on graphene, 2D layered materials that exhibit a flat surface, but without dangling bonds, have generated a great amount of interest for fundamental and practical applications of SERS. Seo et al.<sup>126</sup> demonstrated a graphene/rhenium oxide sulfide (ReO<sub>x</sub>S<sub>y</sub>) vertical heterostructure as an ultrasensitive SERS platform. The enhanced electron transfer and exciton resonances improve the Raman detection limit to the level of 10<sup>-12</sup> mol/L (Figure 8a–c).

Molybdenum disulfide (MoS<sub>2</sub>) is a typical 2D TMD, consisting of a Mo monolayer sandwiched between two S layers. Ling et al.<sup>127</sup> observed that the copper phthalocyanine molecule enhances the higher-frequency phonon modes on MoS<sub>2</sub>, although the enhancement is much weaker than those on graphene and h-BN. The SERS signal on MoS<sub>2</sub> can be improved by more than 1 order of magnitude when surface defects are introduced via plasma treatment (Figure 8d,e).<sup>128</sup> It is suggested that the defects create local dipoles, which enhance the charge transfer between probe molecules and MoS<sub>2</sub>. The underlying factor for the chemical enhancement is, in some measure, the electron transition probability rate, which depends on the density of electronic states. The phase transition of MoS<sub>2</sub> from the semiconducting 2H-phase (with trigonal-prismatic coordination) to the metallic 1T-phase (with octahedral structure) facilitates electron transfer from the

Fermi level of MoS<sub>2</sub> to the highest occupied molecular orbital of the probe molecules and increases the SERS signal as a result.<sup>129</sup> In addition to MoS<sub>2</sub>, SERS has been reported on some other 2D TMDs, such as WS<sub>2</sub>,<sup>130</sup> NbS<sub>2</sub>,<sup>131</sup> MoSe<sub>2</sub>,<sup>129</sup> WSe<sub>2</sub>,<sup>132</sup> MoTe<sub>2</sub>, and WTe<sub>2</sub>.<sup>133</sup> The tunable electronic structures of TMDs via the atomic arrangement and composition variation provide abundant models to understand the fundamentals of chemical enhancement.

MXene is a young family of 2D materials, which was first reported in 2011 by Gogotsi and co-workers.<sup>134</sup> It represents the transition metal carbides, carbonitrides, or nitrides with the general formula of M<sub>n+1</sub>X<sub>n</sub>T<sub>x</sub> ( $n = 1, 2, \text{ or } 3$ ), where M is an early transition metal, X is carbon and/or nitrogen, and T refers to the surface termination, such as OH, O, or F groups. MXene exhibits unique electronic and optical properties, including metallic conductivity and plasmon resonance in the visible and near-infrared range. Titanium carbide MXene (Ti<sub>3</sub>C<sub>2</sub>T<sub>x</sub>) can be used to detect several dyes with calculated EFs up to 10<sup>6</sup> (Figure 8f,g).<sup>135</sup> Titanium nitride MXene (Ti<sub>2</sub>NT<sub>x</sub>), which is drop-casted on paper, silicon, and glass-based substrates, enables the single-molecule detection of R6G at the 532 nm excitation wavelength.<sup>136</sup>

The state-of-the-art nonmetallic 2D materials shed new light on the practical applications of SERS due to their specific advantages. They have atomically layered structures with a high specific surface area. Their mechanical, chemical, and thermal stability are comparable to or higher than those of metallic substrates. For most of the isolated nonmetallic 2D SERS substrates, the chemical enhancement, which originates from the charge transfer between target molecules and the substrate, plays a significant role in SERS.<sup>137</sup> A very recent work<sup>16</sup> demonstrated that the EF of CM can reach ~10<sup>6</sup>, which is several orders of magnitude lower than that of EM on coinage metal substrates. Even so, nonmetallic 2D materials are

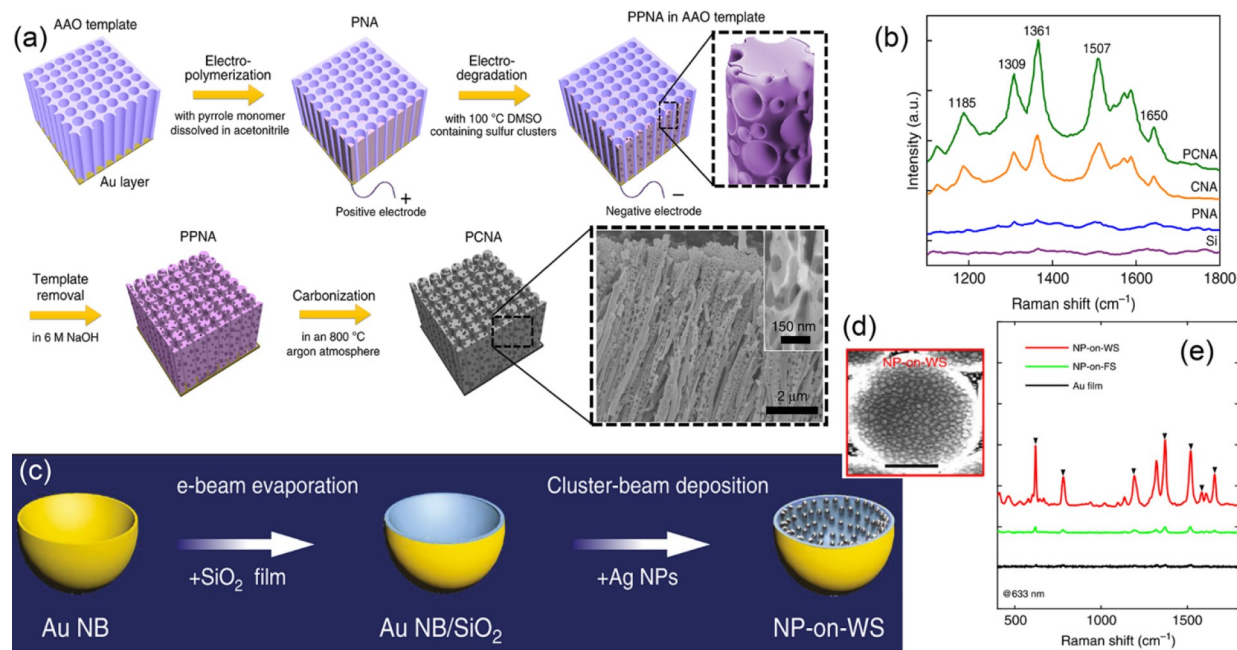


**Figure 9.** (a) Scheme of steps for synthesizing the PCNA. The bottom right inset shows an SEM image of the PCNA and an enlarged SEM image of a single porous carbon nanowire. (b) Measured Raman spectra of R6G molecules at a concentration of 10 μM on various substrates. (c) Fabrication process of hierarchical nanostructures of nanoparticles on warped substrate (NP-on-W). (d) SEM image of a NP-on-W; the scale bar represents 500 nm. (e) SERS spectra for R6G on various substrates. Panels (a,b) were adapted with permission under a Creative Commons CC BY license from ref 16. Copyright 2020 The Authors. Panels (c–e) were adapted with permission under a Creative Commons CC BY license from ref 167. Copyright 2018 The Authors.

identified as potential SERS substrates with highly tunable sensitivity and selectivity, and many strategies have been proposed to increase the EF via the modifications of composition and morphology, and the formation of heterostructures. Valeš et al.<sup>138</sup> reported that fluorinated and 4-nitrophenyl-functionalized graphene have EFs higher than those of pristine graphene, and the relative enhancement increases along with the increase of the doping level of functional groups. The formation of defects or functional groups on graphene using ultraviolet or ozone oxidation enables the Raman enhancement by 3 orders of magnitude.<sup>139</sup> The heterostructures of 2D materials formed by layer-by-layer stacking with an arbitrary sequence have modified density of states. Tan et al.<sup>140</sup> used WSe<sub>2</sub> monolayer (W) and graphene (G) to construct heterostructures with different stacking sequences, including G/W, W/G, G/W/G/W, and W/G/G/W. The intensity of Raman radiation is much stronger on the heterostructures as compared with that on homogeneous layers, and the EFs depend on the stacking sequence, following the order of  $G/W > G/W/G/W > G > W/G \sim W/G/G/W > W$ .

The heterogeneous structures of nonmetallic 2D materials and coinage metal nanomaterials have combined enhancement from CM and EM. Lu et al.<sup>141</sup> decorated ultrathin MoS<sub>2</sub> films selectively with Au nanoparticles and used this hybrid SERS substrate to detect nonthiolated aromatic molecules. The strong SERS signal of aromatic molecules is assigned to the collective effects of the efficient adsorption of the molecules onto MoS<sub>2</sub> and the strong coupling of the Au nanoparticles to the SERS. Wang et al.<sup>142</sup> demonstrated that a graphene/Au nanopyramid hybrid system can boost a high density of hot spots with local SERS EF over 10<sup>10</sup>, enabling label-free single-molecule detection. The addition of graphene allows the determination of chemical enhancement and electromagnetic

enhancement, separately, in a semiquantitative mode. The chemically inert 2D material covers metal nanostructures to protect them from contamination and to improve the stability and repeatability of the substrate. Liu et al.<sup>143</sup> reported monolayer graphene shielded periodic Ag nanostructures as long-term stable SERS substrates. The monolayer graphene acts as a corrosion barrier, which alleviates both the chemical corrosion and the photoinduced damage.

The above discussions have convincingly shown that 2D materials can bring about several advantages for SERS. These include the selectivity to some specific molecules, such as nonthiolated aromatic molecules, and the possibility of combining enhancements from both CM and EM. Some 2D materials are chemically inert, so that they can be used as coatings to stabilize metallic SERS substrates.

## 6. SERS SUBSTRATE MADE FROM 3D NANOSTRUCTURES

Three-dimensional SERS substrates allow the construction of SERS active sites in 3D space. SERS substrates made from 3D nanostructures have particular advantages, such as high effectiveness for the utilization of lasers within a 3D laser confocal region and high sensitivity for highly diluted target molecules.<sup>144,145</sup> Several physical and chemical methods have been utilized to create 3D SERS substrates. The strategies are generally classified into template-assisted fabrication,<sup>146,147</sup> bottom-up assembly,<sup>148,149</sup> and top-down fabrication.<sup>150</sup>

### 6.1. Template-Assisted Fabrication

Template-assisted fabrication provides a reproducible pathway for preparing well-defined nanostructures. Polystyrene micro/nanospheres,<sup>151</sup> block copolymers,<sup>152</sup> AAO,<sup>153,154</sup> and porous silica<sup>155</sup> are typical templates, which constrain the growth of nanostructures in their pores or gaps. More complex structures

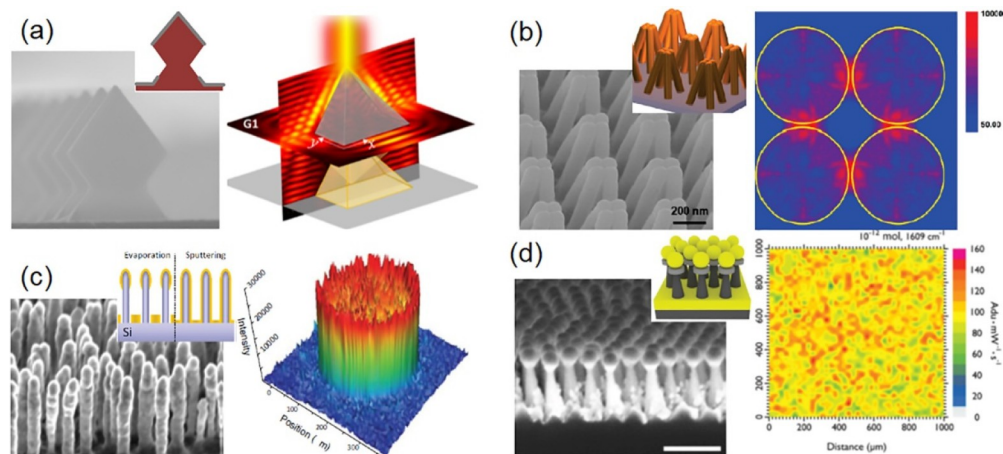


**Figure 10.** (a) Scheme and SEM image of 3D Ag mirror-like micropylar structures and the intensity of the electric field near the structure. (b) Scheme and SEM image of closed Au nanofingers and the distribution of electric field intensity for the four Au spheres of 68 nm radius. (c) Scheme and SEM image of Ag lumps at the top of the Si pillars and 3D representation of the Raman map. (d) Scheme and SEM image of Au nanoparticles on nanohoodoos and the Raman map. Panel (a) was adapted with permission from ref 184. Copyright 2020 Springer-Verlag GmbH Austria. Panel (b) was adapted from 179. Copyright 2010 American Chemical Society. Panel (c) was adapted with permission from 186. Copyright 2012 Wiley-VCH Verlag GmbH & Co. KGaA, Weinheim. Panel (d) was adapted with permission from 191. Copyright 2018 Wiley-VCH Verlag GmbH & Co. KGaA, Weinheim.

have been innovated recently using various templates and deposition methods. Guan et al.<sup>156</sup> constructed “hedgehog-like” Ag nanocone arrays with the assistance of polystyrene microsphere and nanosphere binary layers. Compared with conventional planar nanocone arrays and 3D nanosphere arrays, these hedgehog-like nanocone arrays enable the effective utilization of light and provide more hot spots at the tips, resulting in a more stable and stronger SERS signal. Chen et al.<sup>157</sup> deposited Au–Ag alloys electrochemically in the through holes of AAO templates for nanopillar arrays. In order to create more hot spots on the nanopillars, they dissolved Ag atoms chemically from the Au–Ag alloys and then redeposited Ag atoms on the porous Au nanopillar. The 3D porous Au@Ag nanopillar arrays exhibit SERS sensitivities much higher than those of solid Au nanopillars, and this porous structure enables the adsorption and detection of polychlorinated biphenyls, which is known as nonadsorbing molecules for metallic SERS substrates. Ultrathin AAO films with tunable pore size and wall thickness are used as masks for the fabrication of Ag nanoparticle arrays.<sup>158</sup> The ultrathin masks allow the large-scale production of closely packed Ag nanoparticle arrays with a high density of hot spots. Mesoporous molecular sieves with specific mesoporous structures are used as templates for the synthesis of nanostructured SERS substrates.<sup>159</sup> Chen et al.<sup>16</sup> deposited polypyrrole electrochemically into the pores of AAO templates and generated porous carbon nanotube arrays (PCNAs) via the electro-degradation at 100 °C in a dimethyl sulfoxide solution and thermal annealing at 800 °C under an argon atmosphere (Figure 9a). The metal-free PCNA substrate provides not only high signal enhancement ( $\sim 10^6$ ) due to its strong broadband CTR for large chemical enhancement but also extraordinarily high reproducibility or sample-to-sample and time-to-time consistency in the SERS spectrum, due to the absence of electromagnetic hot spots (Figure 9b). In addition to AAO, silica KIT-6 has an interpenetrating cylindrical pore system, which allows the formation of a Ag mesh structure via a nanocasting process. Silica SAB-15 consists of parallel hexagonal pores, shaping the chemically deposited Ag as nanowire bundles.

Some 3D structures or arrays, such as fibrous membranes,<sup>160</sup> melamine sponge block copolymers,<sup>161</sup> nanocellulose,<sup>162</sup> carbon nanotube arrays,<sup>163</sup> TiO<sub>2</sub> nanotube arrays,<sup>164</sup> and ZnO micron rods,<sup>165</sup> are used as templates as well for supporting plasmonic nanoparticles on the surface. The customized size, shape, or interstice of templates allows precise geometric control and positional arrangement of plasmonic nanoparticles for a strong SERS signal. For most templates, nanostructures with convex topography, such as acute tips or pillars, create hot spots within a tiny region, lowering the probability for the approach and adsorption of analyte molecules on the active sites. Thus, high sensitivity is always accompanied by a long preparation time for analyte accumulation, which hinders the time response.<sup>166</sup> Mao et al.<sup>167</sup> employed Au nanobowl arrays, which have concave topography, as templates to support SERS active Ag nanoparticles (Figure 9c,d). Experiments for single-molecule detection with a short soaking time are realized in conjunction with broadband response and uniformity (Figure 9e). The manipulation of hot spots in a warped spatial geometry provides a new design platform for broadband and huge field enhancements.

## 6.2. Bottom-Up Assembly

The bottom-up plasmonic assemblies refer to the SERS active structures generated via a synthetic combination of plasmonic building blocks. Plasmonic core–satellite structures, which consist of a bigger particle at the center serving as a core, and some smaller particles encircling the core as satellites provide in-built hot spots for excellent SERS probing.<sup>168</sup> Mueller et al.<sup>169</sup> synthesized 3D nanoparticle supercrystals via the self-assembly of Au nanoparticles on a liquid subphase for excellent structural order and small interparticle gaps. Thiolated polystyrene molecules functionalize the Au nanoparticles, stabilize the supercrystals, and act as spacers between the nanoparticles to form nanogaps with the width of 1–4 nm. The near-field inside the supercrystal within the framework of plasmon polaritons form due to strong light–matter interaction. The intensity of SERS is uniform within 10% across the supercrystal with a peak integrated enhancement of

up to 300 and a peak hot spot enhancement of  $10^5$ . Metal–organic frameworks (MOFs) are used as host matrices for in situ growth of Au nanoparticles.<sup>170</sup> The Au nanoparticle-embedded MOF nanocomposites combine the LSPR properties of Au nanoparticles and the high adsorption capability of MOF, making them highly sensitive SERS probes. A SERS detection limit of  $10^{-12}$  mol·L<sup>-1</sup> for R6G and benzidine has been demonstrated. Hierarchical flower-like Au microstructures are synthesized via electrochemical deposition.<sup>171</sup> The deposition current and electrolyte concentration, rather than templates and surfactants, are used to adjust the morphology of the hierarchical structure. The microstructures assembled with nanoflakes or nanotips have high densities of hot spots at interstices and tips, enabling the detection limit down to  $10^{-10}$  mol·L<sup>-1</sup>.

### 6.3. Top-Down Fabrication

The top-down fabricated 3D SERS substrates refer to well-defined metal-coated nanostructures prepared by a top-down fabrication process. In all top-down fabricated structures, nanopillar arrays with their top and/or base coated by SERS active metals enable large SERS EFs due to their multidimensional architectures with a large surface area.<sup>172,173</sup> Many methods have been developed for the fabrication of nanopillar arrays for SERS applications, including NSL,<sup>174,175</sup> EBL,<sup>176,177</sup> nanoimprinting lithography,<sup>178,179</sup> maskless reactive ion etching,<sup>180,181</sup> and block copolymer lithography (BCL).<sup>182,183</sup>

NSL and EBL allow the precise control of the geometry of substrates and subsequent plasmonic responses. Apart from cylindrical nanopillars, more complex structures with precisely controlled geometric dimensions have been innovated in recent years. Lafuente et al.<sup>184</sup> fabricated 3D Ag mirror-like micropylamidal structures extending in the *z*-direction by up to 3.7 or 7.7 μm using Si-based EBL (Figure 10a). The periodic Ag micropylamids are employed for SERS mapping in a large area, and the SERS signals are averaged in the whole area, resulting in a low relative standard deviation value for the  $10^{-6}$ – $10^{-9}$  mol·L<sup>-1</sup> concentration range of target molecules. Tandem Au–SiO<sub>2</sub>–Au nanocone arrays fabricated with EBL can provide a 10 times higher SERS intensity when compared with periodic Au nanocone arrays.<sup>185</sup> The disadvantage of EBL is the high fabrication cost due to inherent low throughput in a serial processing tool. Thus, EBL is inadequate for mass production of large areas of nanostructures.

Some alternatives have been developed for top-down fabrication of 3D SERS substrates. Hu et al.<sup>179</sup> prepared Au-coated nanoscale polymer fingers using the nanoimprinting technique (Figure 10b). The nanofingers are flexible, and their tips can be brought together to trap molecules, while the Au-coated fingertips form hot spots for molecule detection based on SERS. Schmidt et al.<sup>186</sup> used a maskless reactive ion etching process to fabricate Si nanopillars and then deposited Ag partially or conformally onto the Si nanopillars (Figure 10c). This work demonstrated the possibility of simple, reliable, and reproducible large-scale fabrication of analyte trapping SERS substrates using standard Si processing equipment, and this technique has been successfully commercialized by the startup company SILMECO.

BCL is an emerging technology for the large-scale production of nanosized templates.<sup>187–189</sup> Nanocavities can be generated by the microphase separation of block copolymers. The incorporation of inorganic etching resists into the block copolymer mask facilitates the production of

nanostructures made from a variety of materials.<sup>190</sup> Akinoglu et al.<sup>182</sup> developed a SERS sensing template, consisting of a perforated Au film at the base of the nanopillars and Au dots on top of the nanopillars via BCL. The coupling between the Au dot array and perforated Au film at the base of the nanopillars significantly increased the SERS efficiency. The easy, scalable, and cost-effective method is capable of producing SERS substrates with average EFs as high as  $10^7$ , and the relative standard deviation of the block-copolymer-derived templates is only 8% in the measurement of the Raman intensity. Wu et al.<sup>191</sup> innovated a SERS substrate consisting of Au nanoparticles that can slide and aggregate on Al<sub>2</sub>O<sub>3</sub>/Si nanohoodoos (Figure 10d). It is worth mentioning that the nanohoodoos, which are fabricated using wafer-scale BCL, can be recycled after SERS analyses by complete removal of Au via a wet etching process without compromising performance.

## 7. SERS SUBSTRATE IN 4D SPACE AND TIME DOMAINS

The rapid development of nanotechnology has greatly accelerated the innovation of SERS substrates with a large surface area, a high density of SERS hot spots, and a specific nanostructure to trap target molecules. Although state-of-the-art SERS substrates have successfully met some analytic requirements of sensitivity, stability, and reproducibility, there are still many challenges in the understanding, development, implementation, and application of SERS techniques. Many important questions await appropriate answers: Can any enhanced Raman scattering phenomenon, which cannot be explained by the EM, be explained by the CM? Can the functionality of hot spots be clarified? Can the theoretical calculation of EFs be more accurate? These questions require the further development of the SERS theory. Experimentally, it is of vital importance to determine the dynamic process of the capture of target molecules at hot spots, clarify the combination of EM and CM for the giant SERS EFs, and further push up the spatial resolution limit for SERS as applied to scanning probe microscopy. In a relatively new frontier of Raman spectroscopy, it is of great interest to improve the SERS resolution in the time domain as well as in the spatial domain, either separately or collectively, and explore the application of such a powerful Raman spectroscopy technology to solve some critical problems in chemistry and biology.

### 7.1. Subsecond Temporal Resolution

Conventional time-resolved SERS (TR-SERS) operates with a continuous-wave laser and detects spontaneous Raman scattering. It captures Raman spectra continuously during a dynamic process, so that it is capable of identifying the change of molecular structures and determining reactive intermediates or transient states on the SERS active surface. Liu and co-workers<sup>192,193</sup> innovated a TR-SERS strategy, which is based on the dynamic agglomeration of Ag nanoparticles in their colloidal suspension during solvent evaporation. The dynamic adjustment of the interparticle distance during the transition process enables a significant enhancement of the SERS signal at some time point, making it a universal method for in situ detection of chemical residuals. Fujita et al.<sup>194</sup> performed TR-SERS to observe the position and spectra of Au nanoparticles simultaneously in living cells with high spatial and temporal resolutions. The subsecond TR-SERS provides the information on the transportation of Au nanoparticles on the cell surface

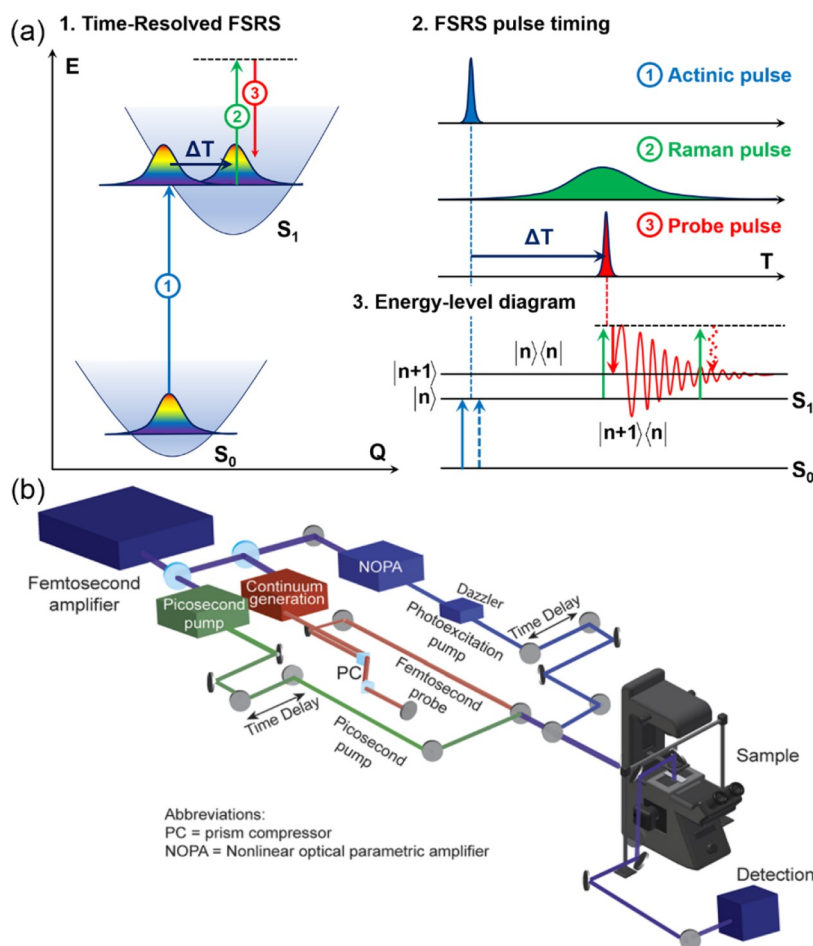


**Figure 11.** (a) Schematic representation of time-resolved FSRs. A femtosecond pump pulse promotes the system to an excited electronic state. The structural evolution is probed by Raman and probe pulses driving stimulated Raman transitions after a variable time delay,  $\Delta T$ . Bra-ket energy-level diagram depicting the FSRS process. (b) Schematic illustration of an FSRS setup with an integrated microscope for super-resolution Raman imaging. Part (b) was adapted from ref 208. Copyright 2016 American Chemical Society.

and in the cell, which can be linked to the molecular signatures of biological activities at distinct locations.

The in-depth understanding of catalytic processes in photo/electrochemical energy conversion is strongly driven by the global energy and environmental challenges. TR-SERS is capable of determining catalyst states, surface transformation, and interfacial intermediates under operando conditions and provides insights regarding the reaction kinetics.<sup>195,196</sup> Weckhuysen and co-workers<sup>197</sup> took advantage of the characteristics of Cu, which acts both as an active  $\text{CO}_2$  reduction reaction ( $\text{CO}_2\text{RR}$ ) electrocatalyst and SERS active substrate to achieve subsecond TR-SERS under  $\text{CO}_2\text{RR}$  conditions. The investigation reveals the dynamic Cu surface reconstruction as well as chemical processes of adsorbed CO species on polycrystalline Cu electrodes during  $\text{CO}_2\text{RR}$ . Dong et al.<sup>198</sup> distributed  $\text{Au}@\text{SiO}_2$  shell-isolated nanoparticles on smooth Pt(*hkl*) electrode surfaces and employed in situ electrochemical SERS to examine the oxygen reduction reaction (ORR) process at the Pt(*hkl*) surface. Direct spectroscopic evidence for ORR intermediates indicates that, under acidic conditions, the pathway of ORR at Pt(111) occurs through the formation of  $\text{HO}_2^*$ , whereas at Pt(110) and Pt(100), it occurs via the generation of  $\text{OH}^*$ . Single-layer  $\text{MoS}_2$ -coated polyhedral Ag heterostructures ( $\text{Ag}@\text{MoS}_2$ ) are used as bifunctional substrates, i.e., electrocatalytic  $\text{MoS}_2$

surfaces for hydrogen evolution reaction (HER) and plasmonic Ag core for the real-time SERS.<sup>199</sup> Raman spectroscopic results prove the S–H bonding formation on the  $\text{MoS}_2$  surface during the HER process, suggesting that the S atom of  $\text{MoS}_2$  is the catalytic active site for the reaction. Radjenovic and Hardwick<sup>200</sup> used the Raman active bands of superoxide ( $\text{O}_2^*$ ) for probing the influence of electrolyte on the ORR in non-aqueous electrolytes and intermediates at the electrode surface. The TR-SERS enables the real-time observation of the flux and reorientation of ions at the electrode/electrolyte interface.

SERS boosts the sensitivity toward adsorbed species, enabling shorter spectrum acquisition time for a good signal/noise ratio, but the temporal resolution of the conventional TR-SERS, which is normally in the range from subsecond to several tens of seconds, is still too poor to monitor the ultrafast dynamics of atomic bond making or breaking on the picosecond time scale.<sup>201</sup> Thus, the spectroscopic results from conventional TR-SERS provide some evidence for the analysis of reaction mechanism and kinetics, but the dynamic information is still missing. Theoretical calculations are usually required to complete the story.<sup>198,202,203</sup>

## 7.2. Femtosecond Temporal Resolution

Femtosecond stimulated Raman spectroscopy (FSRS) enables the measurement of vibrational structural information with a

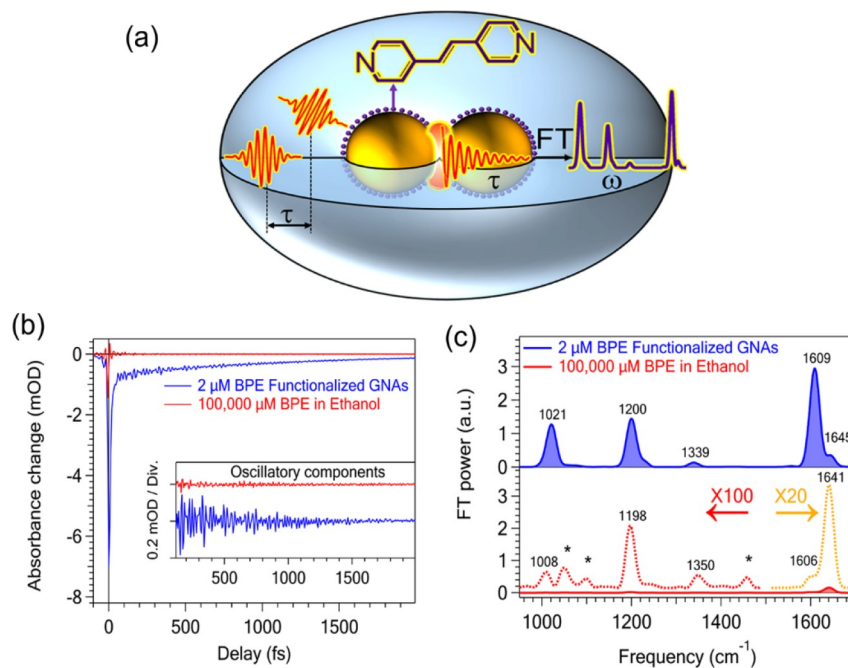


**Figure 12.** (a) Schematic illustration of SE-ISRS for BPE functionalized Au nanoparticle assemblies. (b) Pump–probe signals of 0.1 M BPE in ethanol (red) and the 2  $\mu\text{M}$  BPE-functionalized Au nanoparticle assemblies in water (blue). Their oscillatory components are shown in the inset. (c) Fourier transform power spectra of the oscillatory components shown in the inset of (b). Adapted from ref 214. Copyright 2020 American Chemical Society.

time resolution comparable to or faster than that of the oscillatory period of nuclear motions.<sup>204</sup> This technique originates from the ultrafast pump–probe spectroscopy.<sup>205</sup> Yoshizawa et al.<sup>206</sup> reported the first FSRS experiment in 1994. Since then, the three-pulse configuration has been widely used in FSRS experiments. An actinic pump pulse excites the molecule to an instantaneous state, and then the structure information is read out at various time delays by a sequence of a narrowband Raman pump pulse and a broadband probe pulse (Figure 11a). The probe pulse generates a macroscopic polarization with high time precision, creating a free induction decay, which is measured by a dispersed detection system.<sup>207</sup> Silva et al.<sup>208</sup> demonstrated the super-resolution Raman microscopy, which is based on the combination of stimulated emission depletion microscopy and FSRS. They utilized a kilohertz femtosecond amplifier, of which the output is split into three beams. These beams are focused onto the sample with an inverted microscope, and the signal is collected in transmission mode with a condenser utilized for collimation (Figure 11b). A toroidal-shaped decoherence pulse is used to eliminate the vibrational signal from the edges of the focal spot, improving the spatial resolution of the microscope beyond the diffraction limit.

Pellatz et al.<sup>209</sup> used pump–probe Raman scattering to investigate the apical oxygen vibration in  $\text{YBa}_2\text{Cu}_3\text{O}_{6+x}$  under non-equilibrium conditions and find that hot and cold phonons are out of thermal equilibrium, but electrons and hot phonons are at or near thermal equilibrium at time delays below 1 ps. The time dependence of phonon population demonstrates strong electron–phonon coupling. Zhu et al.<sup>210</sup> investigated the excitonic population dynamics of carbon nanotubes confined in long linear carbon chains. The exciton relaxation dynamics of the confined carbon chains occurs at hundreds of picoseconds, in strong contrast to the dynamics of a nanotube host that occurs in a few picoseconds. The strong

coupling between the chain and the nanotube host provides clear evidence for an efficient energy transfer from the host nanotube to the chain. Mathies and co-workers<sup>211</sup> reported the time-resolved FSRS spectra of a charge transfer excited noncovalent complex tetracyanoethylene/1-chloronaphthalene (TCNE/CIN) in dichloromethane (DCM) with a time resolution of 40 fs. FSRS enables the observation of fundamental vibrations including the in-plane bending of the TCNE cyano groups and the symmetric stretch of the central C=C bond in TCNE<sup>•-</sup>. The impulsive stimulated Raman measurements of the complex provide the information on the DCM solvent shell, the out-of-plane bending of TCNE, as well as the frequency shift due to the proximity of the contact ion pairs. The structural and vibrational time evolution of the key vibrational modes of the TCNE/ $\pi$ /CIN molecular complex, which is investigated by adiabatic molecular dynamic simulations, agrees well with the experimental results, unveiling a correlation between vibrational fingerprints and electronic properties.<sup>212</sup>

FSRS provides a sufficiently detailed and time-resolved vibrational signal of the electronically excited molecular complex, thus it is a powerful approach for revealing the real-time nuclear dynamics that makes up a multidimensional polyatomic reaction coordinate.<sup>213</sup> In fact, the work combining SERS and coherent nonlinear time-resolved Raman spectroscopy has been reported. Kumar et al.<sup>214</sup> combined surface-enhanced Raman scattering with the coherent nonlinear Raman technique and made it a promising route for achieving higher sensitivity and time-resolved SERS measurements. They also reported time domain Raman measurements of *trans*-1,2-bis(4-pyridyl)ethylene (BPE) adsorbed on Au nanoparticle assemblies, which are carried out with impulsive stimulated Raman spectroscopy using sub-8 fs pulses (Figure 12a). They observed coherent nuclear wave packet motion of BPE on Au nanoparticle assemblies with drastic enhancement through the

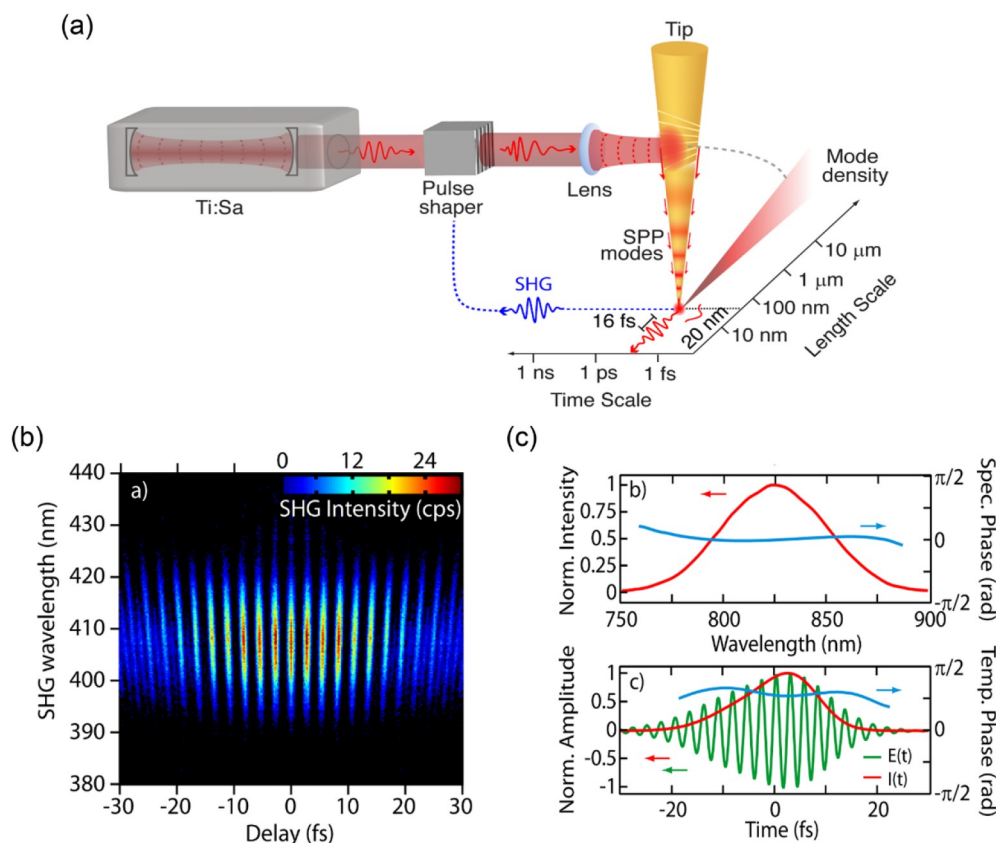


**Figure 13.** (a) Micro-to-nanoscale optical mode transformation on a tip. (b) Frequency-resolved optical gating measurement based on apex-localized second harmonic generation of adiabatically nanofocused SPP. (c) Multiphoton intrapulse interference phase scan optimization for flat spectral phase yields a nearly transform-limited 16 fs pulse for a 60 nm fwhm bandwidth. Adapted with from ref 233. Copyright 2011 American Chemical Society.

surface plasmon resonance, which provides information on the Raman active vibrations in the time domain (Figure 12b). Through Fourier transform of the measured time domain Raman data, they obtained the SERS spectra of BPE and found an EF as high as  $10^5$ – $10^6$  (Figure 12c). This study not only demonstrates the applicability of time domain nonlinear Raman techniques in SERS, i.e., surface-enhanced impulsive stimulated Raman spectroscopy (SE-ISRS),<sup>215</sup> but also provides a technical basis for femtosecond time-resolved SE-ISRS experiments to track ultrafast dynamics of the adsorbates.<sup>216</sup>

### 7.3. Nanometer Spatial Resolution

Scanning probe microscopy (SPM) provides scientists with a powerful tool to investigate surfaces with atomic resolution.<sup>217</sup> On the basis of SPM techniques, Wessel<sup>218</sup> proposed the concept of surface-enhanced optical microscopy (SEOM) based on optical field confinement by surface plasmons of a sub-micrometer-sized metal probe. The tip of the metal probe serves as an antenna that receives an incoming optical field and propagates the field to a nearby sample surface for interactions. The induced surface polarization is reradiated by the tip, thereby generating a Raman spectrum. The SEOM has a spatial resolution unlimited by optical diffraction effects, and its detection sensitivity approaching 1 nm is projected.<sup>195</sup> Nowadays, this technique is widely known as TERS, which was successfully demonstrated in the early 2000s by several groups.<sup>219–221</sup> In the past two decades, the spatial resolution

of TERS has been improved from several tens of nanometers to a few nanometers.<sup>46</sup>

One of the major topics in TERS is the efficient collection and delivery of electromagnetic energy to the minuscule region of interest. In conventional TERS, surface plasmons are excited on the metallic probe via directly focusing the laser beam in the vicinity of the tip apex.<sup>222</sup> The mismatch between the mode volumes of a far-field optical mode and the highly confined plasmonic mode leads to very small overlap of the electromagnetic field, resulting in low coupling efficiency.<sup>223</sup> Tapered structures allow for the concentration of surface plasmons at the apex of the convergent geometries.<sup>220,224</sup> The 3D tapered cones enable the efficient coupling of the far-field radiation to the near-field region, which leads to the significant increase of local field by 3 orders of magnitude in intensity.<sup>225</sup> Ropers et al.<sup>226</sup> scribed 1D gratings onto the tip shaft of 3D tapered cones with apex radii of a few tens of nanometers and demonstrated an efficient propagation of SPPs over more than  $10\ \mu\text{m}$  along the tip shaft toward the cone apex. The grating-coupled conical tips serve as bright nanoscale light sources for nearly background-free scattering-type scanning near-field optical microscopy. The dipolar nanoemitter allows around 20 nm spatial confinement, which is more than 1 order of magnitude beyond the optical diffraction limit.<sup>43</sup>

### 7.4. High Spatiotemporal Resolution

FSRS can probe the ultrafast dynamics of molecules, but it does not intrinsically have spatial resolution beyond the optical diffraction limit. In contrast, TERS is capable of achieving the

vibrational spectra of adsorbates with a spatial resolution in nanometer scales. However, relatively few efforts have focused on the incorporation of ultrafast spectroscopic techniques with TERS.<sup>227</sup> Several groups have demonstrated advances of time-resolved TERS. Kawata and co-workers<sup>228</sup> reported the tip-enhanced coherent anti-Stokes Raman scattering (CARS) of adenine molecules in a nanometric DNA network. The excitation of the CARS polarization is extremely confined to the tip apex, resulting in a resolution far beyond the optical diffraction limit. The tip-enhanced CARS image is recorded in 100 ms for one pixel. Van Duyne and co-workers coupled an optical parametric oscillator with a TERS microscope to excite the tip plasmon with picosecond excitation source and performed the TERS measurements in ambient conditions<sup>229</sup> and in ultrahigh vacuum (UHV).<sup>227</sup> They demonstrated that picosecond TERS of a resonant adsorbate can be observed in UHV without the permanent loss of signal that plagues picosecond TERS in ambient conditions. Although these authors do not achieve the spatially and temporally resolved dynamics of surface-bound molecules, their findings suggest that a UHV environment for time-resolved TERS experiments is a valuable asset.

Wickramasinghe et al.<sup>230</sup> introduced a collinear, tunable stimulating beam along with a polarization-modulated pump beam into a conventional TERS setup and obtained a stimulated TERS image of azobenzene thiol molecules grafted onto Au(111). The signal and the signal-to-noise ratio in TERS are significantly enhanced using the stimulated emission scheme. However, the imaging rate in this work is limited not by the signal acquisition time but rather by the STM scanning rate. Cocker et al.<sup>231</sup> innovated ultrafast terahertz scanning tunneling microscopy (THz-STM), by which a single electron from an individual pentacene molecule's highest occupied molecular orbital is removed within a time window shorter than one oscillation cycle of the terahertz wave, and approximately 100 fs snapshot images of the orbital structure with sub-angstrom spatial resolution are recorded to reveal coherent molecular vibrations at terahertz frequencies directly in the time domain. The dynamics of the energy landscape associated with single electrons and phonons can be traced directly by ultrafast tunneling. Moreover, combining an optical pump pulse with the THz-STM probe will provide access to a multitude of optical excitations. Müller et al.<sup>232</sup> reported the photoemission of sub-10 fs electron pulses from the apex of a Au nanotip driven by the nanofocusing of SPPs and employed the ultrafast electron pulses for point-projection microscopy of an individual nanowire. The spatial resolution reached 20 nm, and the temporal resolution is in the sub-10 fs range. The plasmon-triggered tunneling of femtosecond electron wave packets makes the realization of ultrafast SPM conceivable. Berweger et al.<sup>233</sup> used the same system to demonstrate the continuous micro-to-nanometer self-similar mode matching conversion of the femtosecond SPP field propagating at the apex of the tip to 20 nm space and 16 fs time-limited light pulses (Figure 13).

So far, tracking the intrinsic dynamics of a single molecule directly in the time domain faces many challenges. The integration of pump–probe pulses into TERS is still identified as a valuable pathway to capture the site-specific information about the dynamics of molecules. In the near future, we envisage watching single-molecule movies and chemical reactions in four dimensions.

## 8. SUMMARY AND PERSPECTIVES

This review outlines the efforts made on the dimensional design for SERS, including the most significant strategies for constructing enhancing substrates ranging in structures from 0D to 3D in the past nearly half century. An appropriate SERS substrate identified as highly sensitive, selective, and stable is very much desirable for both basic science and high technology. A SERS technique based on an ideal substrate is versatile for analysis with a high enhancement factor, a good signal reproducibility, and a fast response.

We have shown that, in each category of SERS substrates, design and optimization upon the geometric and composite configuration can be made to achieve an as large as possible enhancement factor of a Raman signal, where both the electromagnetic and chemical enhancement mechanisms can be deeply explored to play active roles. We have also shown that the temporal dimension can be incorporated into SERS by applying femtosecond pulse laser technology so that SERS can be used not only to identify the chemical structure of molecules but also to uncover the ultrafast dynamics of molecule structural changes. Such so-called 4D SERS allows the design and optimization in the geometric configuration of metal nanoparticles and nanostructures and temporal shape of a pulse laser, either separately or collectively.

The ultimate goal for SERS techniques is the capability for measuring structural changes of reacting molecules in nanometer scales and on ultrashort time scales ranging from a few femtoseconds to picoseconds. Tip-enhanced Raman spectroscopy provides a spatial resolution of a few nanometers but lacks temporal information. Femtosecond stimulated Raman spectroscopy enables the measurement of vibrational structural information with a temporal resolution comparable to, or faster than, the oscillatory period of the nuclear motions of molecules. However, there is, so far, no SERS technique which is capable of combining the state-of-the-art spatiotemporal resolutions for deep insights into fundamental problems as to observe the molecule structure change dynamics and, more importantly, while being more difficult to visualize specific chemical reaction dynamics of critical importance.

A critical question is whether dimensional design for SERS could greatly advance the spatiotemporal resolution. Well-designed plasmonic nanostructures with specific shape, size, or alignment can provide highly organized hot spots and thus enable quantitative analysis of single molecules. Here, we suggest the 4D design for SERS, in which the pump–probe process should be planned carefully in accordance with the geometric structures of enhancing substrates, might meet such a fundamental purpose. The incorporation of scanning probe techniques, ultrafast laser pump–probe techniques, and enhancing substrates may create a new pathway to approach the ultimate goal for SERS, as well as for chemical analysis. In the near future, we envisage watching the chemical reactions in four dimensions and visualizing the elementary reaction steps in chemistry.

## ■ AUTHOR INFORMATION

### Corresponding Authors

Wenbo Ju – School of Physics and Optoelectronics, South China University of Technology, Guangzhou 510641, China; [orcid.org/0000-0001-7639-6206](https://orcid.org/0000-0001-7639-6206); Email: [wjuphy@scut.edu.cn](mailto:wjuphy@scut.edu.cn)

Zhiyuan Li – School of Physics and Optoelectronics, South China University of Technology, Guangzhou 510641, China; Email: [phzyli@scut.edu.cn](mailto:phzyli@scut.edu.cn)

## Authors

Li Long – School of Physics and Optoelectronics, South China University of Technology, Guangzhou 510641, China

Hai-Yao Yang – School of Physics and Optoelectronics, South China University of Technology, Guangzhou 510641, China

Complete contact information is available at:

<https://pubs.acs.org/10.1021/acsmaterialsau.2c00005>

## Author Contributions

†L.L. and W.J. contributed equally.

## Notes

The authors declare no competing financial interest.

## ACKNOWLEDGMENTS

The authors are grateful for the financial support from the National Natural Science Foundation of China (12104164, 11974119, and 91850107), Guangdong Innovative and Entrepreneurial Research Team Program (2016ZT06C594), National Key R&D Program of China (2018YFA 0306200), and Science and Technology Project of Guangdong (2020B010190001).

## REFERENCES

- (1) Raman, C. V.; Krishnan, K. S. A new type of secondary radiation. *Nature* **1928**, *121*, 501–502.
- (2) Cui, L.; Ren, X.; Yang, X.; Wang, P.; Qu, Y.; Liang, W.; Sun, M. Plasmon-driven catalysis in aqueous solutions probed by SERS spectroscopy. *J. Raman Spectrosc.* **2016**, *47*, 877–883.
- (3) Wright, D.; Lin, Q.; Berta, D.; Földes, T.; Wagner, A.; Griffiths, J.; Readman, C.; Rosta, E.; Reisner, E.; Baumberg, J. J. Mechanistic study of an immobilized molecular electrocatalyst by in situ gap-plasmon-assisted spectro-electrochemistry. *Nat. Catal.* **2021**, *4*, 157–163.
- (4) Hu, Y.; Cheng, H.; Zhao, X.; Wu, J.; Muhammad, F.; Lin, S.; He, J.; Zhou, L.; Zhang, C.; Deng, Y.; Wang, P.; Zhou, Z.; Nie, S.; Wei, H. Surface-enhanced Raman scattering active gold nanoparticles with enzyme-mimicking activities for measuring glucose and lactate in living tissues. *ACS Nano* **2017**, *11*, 5558–5566.
- (5) Han, X. X.; Rodriguez, R. S.; Haynes, C. L.; Ozaki, Y.; Zhao, B. Surface-enhanced Raman spectroscopy. *Nat. Rev. Methods Primers* **2021**, *1*, 87.
- (6) Halvorson, R. A.; Vikesland, P. J. Surface-enhanced Raman spectroscopy (SERS) for environmental analyses. *Environ. Sci. Technol.* **2010**, *44*, 7749–7755.
- (7) Sharma, B.; Frontiera, R. R.; Henry, A.-I.; Ringe, E.; Van Duyne, R. P. SERS: Materials, applications, and the future. *Mater. Today* **2012**, *15*, 16–25.
- (8) Pieczonka, N. P. W.; Aroca, R. F. Single molecule analysis by surface-enhanced Raman scattering. *Chem. Soc. Rev.* **2008**, *37*, 946–954.
- (9) Tian, Z.-Q.; Ren, B. Adsorption and reaction at electrochemical interfaces as probed by surface-enhanced Raman spectroscopy. *Annu. Rev. Phys. Chem.* **2004**, *55*, 197–229.
- (10) Fleischmann, M.; Hendra, P. J.; McQuillan, A. J. Raman spectra of pyridine adsorbed at a silver electrode. *Chem. Phys. Lett.* **1974**, *26*, 163–166.
- (11) Jeanmaire, D. L.; Van Duyne, R. P. Surface Raman spectroelectrochemistry: Part I. heterocyclic, aromatic, and aliphatic amines adsorbed on the anodized silver electrode. *J. Electroanal. Chem. Interfacial Electrochem.* **1977**, *84*, 1–20.
- (12) Wang, D.-S.; Chew, H.; Kerker, M. Enhanced Raman scattering at the surface (SERS) of a spherical particle. *Appl. Opt.* **1980**, *19*, 2256–2257.
- (13) Netzer, N. L.; Tanaka, Z.; Chen, B.; Jiang, C. Tailoring the SERS enhancement mechanisms of silver nanowire Langmuir–Blodgett films via Galvanic replacement reaction. *J. Phys. Chem. C* **2013**, *117*, 16187–16194.
- (14) Nie, S.; Emory, S. R. Probing single molecules and single nanoparticles by surface-enhanced Raman scattering. *Science* **1997**, *275*, 1102–1106.
- (15) Le Ru, E. C.; Blackie, E.; Meyer, M.; Etchegoin, P. G. Surface enhanced Raman scattering enhancement factors: A comprehensive study. *J. Phys. Chem. C* **2007**, *111*, 13794–13803.
- (16) Chen, N.; Xiao, T.-H.; Luo, Z.; Kitahama, Y.; Hiramatsu, K.; Kishimoto, N.; Itoh, T.; Cheng, Z.; Goda, K. Porous carbon nanowire array for surface-enhanced Raman spectroscopy. *Nat. Commun.* **2020**, *11*, 4772.
- (17) Campion, A.; Kambampati, P. Surface-enhanced Raman scattering. *Chem. Soc. Rev.* **1998**, *27*, 241–250.
- (18) Xu, H.; Aizpurua, J.; Kall, M.; Apell, P. Electromagnetic contributions to single-molecule sensitivity in surface-enhanced Raman scattering. *Phys. Rev. E* **2000**, *62*, 4318–4324.
- (19) Moskovits, M. Surface-enhanced spectroscopy. *Rev. Mod. Phys.* **1985**, *57*, 783–826.
- (20) Gupta, R.; Dyer, M. J.; Weimer, W. A. Preparation and characterization of surface plasmon resonance tunable gold and silver films. *J. Appl. Phys.* **2002**, *92*, 5264–5271.
- (21) Doron-Mor, I.; Barkay, Z.; Filip-Granit, N.; Vaskevich, A.; Rubinstein, I. Ultrathin gold island films on silanized glass. Morphology and optical properties. *Chem. Mater.* **2004**, *16*, 3476–3483.
- (22) Pieczonka, N. P.; Aroca, R. F. Inherent complexities of trace detection by surface-enhanced Raman scattering. *ChemPhysChem* **2005**, *6*, 2473–2484.
- (23) Stiles, P. L.; Dieringer, J. A.; Shah, N. C.; Van Duyne, R. P. Surface-Enhanced Raman Spectroscopy. *Annu. Rev. Anal. Chem.* **2008**, *1*, 601–626.
- (24) Li, Z.-Y. Mesoscopic and microscopic strategies for engineering plasmon-enhanced Raman scattering. *Adv. Opt. Mater.* **2018**, *6*, 1701097.
- (25) Zhang, C.; Chen, B.-Q.; Li, Z.-Y. Optical origin of subnanometer resolution in tip-enhanced Raman mapping. *J. Phys. Chem. C* **2015**, *119*, 11858–11871.
- (26) Chen, J.; McLellan, J. M.; Siekkinen, A.; Xiong, Y.; Li, Z. Y.; Xia, Y. Facile synthesis of goldsilver nanocages with controllable pores on the surface. *J. Am. Chem. Soc.* **2006**, *128*, 14776–14777.
- (27) Moran, C. H.; Rycenga, M.; Xia, X. H.; Cobley, C. M.; Xia, Y. N. Using well-defined Ag nanocubes as substrates to quantify the spatial resolution and penetration depth of surface-enhanced Raman scattering imaging. *Nanotechnology* **2014**, *25*, 014007.
- (28) Fang, J.; Liu, S.; Li, Z. Polyhedral silver mesocages for single particle surface-enhanced Raman scattering-based biosensor. *Bio-materials* **2011**, *32*, 4877–4884.
- (29) Cheng, L.; Ma, C. S.; Yang, G.; You, H. J.; Fang, J. X. Hierarchical silver mesoparticles with tunable surface topographies for highly sensitive surface-enhanced Raman spectroscopy. *J. Mater. Chem. A* **2014**, *2*, 4534–4542.
- (30) Goh, M. S.; Lee, Y. H.; Pedireddy, S.; Phang, I. Y.; Tjiu, W. W.; Tan, J. M.; Ling, X. Y. A chemical route to increase hot spots on silver nanowires for surface-enhanced Raman spectroscopy application. *Langmuir* **2012**, *28*, 14441–14449.
- (31) Cecchini, M. P.; Turek, V. A.; Paget, J.; Kornyshev, A. A.; Edler, J. B. Self-assembled nanoparticle arrays for multiphase trace analyte detection. *Nat. Mater.* **2013**, *12*, 165–171.
- (32) Frontiera, R. R.; Henry, A. I.; Gruenke, N. L.; Van Duyne, R. P. Surface-enhanced femtosecond stimulated Raman spectroscopy. *J. Phys. Chem. Lett.* **2011**, *2*, 1199–1203.

- (33) McCamant, D. W.; Kukura, P.; Yoon, S.; Mathies, R. A. Femtosecond broadband stimulated Raman spectroscopy: Apparatus and methods. *Rev. Sci. Instrum.* **2004**, *75*, 4971–4980.
- (34) Yampolsky, S.; Fishman, D. A.; Dey, S.; Hulkko, E.; Banik, M.; Potma, E. O.; Apkarian, V. A. Seeing a single molecule vibrate through time-resolved coherent anti-Stokes Raman scattering. *Nat. Photonics* **2014**, *8*, 650–656.
- (35) Zong, C.; Premasiri, R.; Lin, H.; Huang, Y.; Zhang, C.; Yang, C.; Ren, B.; Ziegler, L. D.; Cheng, J. X. Plasmon-enhanced stimulated Raman scattering microscopy with single-molecule detection sensitivity. *Nat. Commun.* **2019**, *10*, 5318.
- (36) Fast, A.; Potma, E. O. Coherent Raman scattering with plasmonic antennas. *Nanophotonics* **2019**, *8*, 991–1021.
- (37) Chang, Y. J.; Castner, E. W. Fast responses from “slowly relaxing” liquids: A comparative study of the femtosecond dynamics of triacetin, ethylene glycol, and water. *J. Chem. Phys.* **1993**, *99*, 7289–7299.
- (38) Heisler, I. A.; Meech, S. R. Low-frequency modes of aqueous alkali halide solutions: Glimpsing the hydrogen bonding vibration. *Science* **2010**, *327*, 857–860.
- (39) Giraud, G.; Karolin, J.; Wynne, K. Low-frequency modes of peptides and globular proteins in solution observed by ultrafast OHDRIKES spectroscopy. *Biophys. J.* **2003**, *85*, 1903–1913.
- (40) Turton, D. A.; Senn, H. M.; Harwood, T.; Laphorn, A. J.; Ellis, E. M.; Wynne, K. Terahertz underdamped vibrational motion governs protein-ligand binding in solution. *Nat. Commun.* **2014**, *5*, 3999.
- (41) Portuondo-Campa, E.; Tortschanoff, A.; van Mourik, F.; Chergui, M. Ultrafast nonresonant response of TiO<sub>2</sub> nanostructured films. *J. Chem. Phys.* **2008**, *128*, 244718.
- (42) Chen, X.; Liu, P.; Hu, Z.; Jensen, L. High-resolution tip-enhanced Raman scattering probes sub-molecular density changes. *Nat. Commun.* **2019**, *10*, 2567.
- (43) Neacsu, C. C.; Berweger, S.; Olmon, R. L.; Saraf, L. V.; Ropers, C.; Raschke, M. B. Near-field localization in plasmonic superfocusing: A nanoemitter on a tip. *Nano Lett.* **2010**, *10*, 592–596.
- (44) Sonntag, M. D.; Pozzi, E. A.; Jiang, N.; Hersam, M. C.; Van Duyne, R. P. Recent advances in tip-enhanced Raman spectroscopy. *J. Phys. Chem. Lett.* **2014**, *5*, 3125–3130.
- (45) Liu, Z.; Ding, S.-Y.; Chen, Z.-B.; Wang, X.; Tian, J.-H.; Anema, J. R.; Zhou, X.-S.; Wu, D.-Y.; Mao, B.-W.; Xu, X.; Ren, B.; Tian, Z.-Q. Revealing the molecular structure of single-molecule junctions in different conductance states by fishing-mode tip-enhanced Raman spectroscopy. *Nat. Commun.* **2011**, *2*, 305.
- (46) Zhang, R.; Zhang, Y.; Dong, Z. C.; Jiang, S.; Zhang, C.; Chen, L. G.; Zhang, L.; Liao, Y.; Aizpurua, J.; Luo, Y.; Yang, J. L.; Hou, J. G. Chemical mapping of a single molecule by plasmon-enhanced Raman scattering. *Nature* **2013**, *498*, 82–86.
- (47) Creighton, J. A.; Blatchford, C. G.; Albrecht, M. G. Plasma resonance enhancement of Raman scattering by pyridine adsorbed on silver or gold sol particles of size comparable to the excitation wavelength. *J. Chem. Soc., Faraday Trans. 2* **1979**, *75*, 790–798.
- (48) Freeman, R. G.; Grabar, K. C.; Allison, K. J.; Bright, R. M.; Davis, J. A.; Guthrie, A. P.; Hommer, M. B.; Jackson, M. A.; Smith, P. C.; Walter, D. G.; Natan, M. J. Self-assembled metal colloid monolayers: An approach to SERS substrates. *Science* **1995**, *267*, 1629–1632.
- (49) Natan, M. J. Surface enhanced Raman scattering. *Faraday Discuss.* **2006**, *132*, 321–328.
- (50) Wang, D.-S.; Kerker, M. Enhanced Raman scattering by molecules adsorbed at the surface of colloidal spheroids. *Phys. Rev. B* **1981**, *24*, 1777–1790.
- (51) Zeman, E. J.; Schatz, G. C. An accurate electromagnetic theory study of surface enhancement factors for silver, gold, copper, lithium, sodium, aluminum, gallium, indium, zinc, and cadmium. *J. Phys. Chem.* **1987**, *91*, 634–643.
- (52) Emory, S. R.; Haskins, W. E.; Nie, S. M. Direct observation of size-dependent optical enhancement in single metal nanoparticles. *J. Am. Chem. Soc.* **1998**, *120*, 8009–8010.
- (53) Kneipp, K.; Kneipp, H.; Manoharan, R.; Hanlon, E. B.; Itzkan, I.; Dasari, R. R.; Feld, M. S. Extremely large enhancement factors in surface-enhanced Raman scattering for molecules on colloidal gold clusters. *Appl. Spectrosc.* **1998**, *52*, 1493–1497.
- (54) Krug, J. T.; Wang, G. D.; Emory, S. R.; Nie, S. M. Efficient Raman enhancement and intermittent light emission observed in single gold nanocrystals. *J. Am. Chem. Soc.* **1999**, *121*, 9208–9214.
- (55) Lyon, L. A.; Keating, C. D.; Fox, A. P.; Baker, B. E.; He, L.; Nicewarner, S. R.; Mulvaney, S. P.; Natan, M. J. Raman spectroscopy. *Anal. Chem.* **1998**, *70*, 341–362.
- (56) Xu, H. X.; Bjerneld, E. J.; Kall, M.; Borjesson, L. Spectroscopy of single hemoglobin molecules by surface enhanced Raman scattering. *Phys. Rev. Lett.* **1999**, *83*, 4357–4360.
- (57) Zhu, Z. H.; Zhu, T.; Liu, Z. F. Raman scattering enhancement contributed from individual gold nanoparticles and interparticle coupling. *Nanotechnology* **2004**, *15*, 357–364.
- (58) Wang, D.-S.; Xie, T.; Li, Y. D. Nanocrystals: Solution-based synthesis and applications as nanocatalysts. *Nano Res.* **2009**, *2*, 30–46.
- (59) Wu, Z.; Yang, S.; Wu, W. Shape control of inorganic nanoparticles from solution. *Nanoscale* **2016**, *8*, 1237–1259.
- (60) Guo, H. Y.; Ruan, F. X.; Lu, L. H.; Hu, J. W.; Pan, J. A.; Yang, Z. L.; Ren, B. Correlating the shape, surface plasmon resonance, and surface-enhanced Raman scattering of gold nanorods. *J. Phys. Chem. C* **2009**, *113*, 10459–10464.
- (61) Nikoobakht, B.; El-Sayed, M. A. Surface-enhanced Raman scattering studies on aggregated gold nanorods. *J. Phys. Chem. A* **2003**, *107*, 3372–3378.
- (62) Zhang, Q.; Li, W.; Moran, C.; Zeng, J.; Chen, J.; Wen, L.-P.; Xia, Y. Seed-mediated synthesis of Ag nanocubes with controllable edge lengths in the range of 30–200 nm and comparison of their optical properties. *J. Am. Chem. Soc.* **2010**, *132*, 11372–11378.
- (63) Santos Costa, J. C.; Ando, R. A.; Sant’Ana, A. C.; Rossi, L. M.; Santos, P. S.; Temperini, M. L. A.; Corio, P. High performance gold nanorods and silver nanocubes in surface-enhanced Raman spectroscopy of pesticides. *Phys. Chem. Chem. Phys.* **2009**, *11*, 7491–7498.
- (64) Haber, J.; Sokolov, K. Synthesis of stable citrate-capped silver nanoprisms. *Langmuir* **2017**, *33*, 10525–10530.
- (65) Pastoriza-Santos, I.; Liz-Marzan, L. M. Synthesis of silver nanoprisms in DMF. *Nano Lett.* **2002**, *2*, 903–905.
- (66) Hou, X.; Wang, Q.; Mao, G.; Liu, H.; Yu, R.; Ren, X. Periodic silver nanocluster arrays over large-area silica nanosphere template as highly sensitive SERS substrate. *Appl. Surf. Sci.* **2018**, *437*, 92–97.
- (67) Silvert, P. Y.; Herrera-Urbina, R.; Duvauchelle, N.; Vijaykrishnan, V.; Elhsissen, K. T. Preparation of colloidal silver dispersions by the polyol process. Part 1—synthesis and characterization. *J. Mater. Chem.* **1996**, *6*, 573–577.
- (68) Kedia, A.; Kumar, P. S. Controlled reshaping and plasmon tuning mechanism of gold nanostars. *J. Mater. Chem. C* **2013**, *1*, 4540–4549.
- (69) Su, Q.; Ma, X.; Dong, J.; Jiang, C.; Qian, W. A reproducible SERS substrate based on electrostatically assisted APTES-functionalized surface-assembly of gold nanostars. *ACS Appl. Mater. Interfaces* **2011**, *3*, 1873–1879.
- (70) Kelly, K. L.; Coronado, E.; Zhao, L. L.; Schatz, G. C. The optical properties of metal nanoparticles: the influence of size, shape, and dielectric environment. *J. Phys. Chem. B* **2003**, *107*, 668–677.
- (71) McLellan, J. M.; Li, Z. Y.; Siekkinen, A. R.; Xia, Y. The SERS activity of a supported Ag nanocube strongly depends on its orientation relative to laser polarization. *Nano Lett.* **2007**, *7*, 1013–1017.
- (72) Orendorff, C. J.; Gole, A.; Sau, T. K.; Murphy, C. J. Surface-enhanced Raman spectroscopy of self-assembled monolayers: Sandwich architecture and nanoparticle shape dependence. *Anal. Chem.* **2005**, *77*, 3261–3266.
- (73) Orendorff, C. J.; Sau, T. K.; Murphy, C. J. Shape-dependent plasmon-resonant gold nanoparticles. *Small* **2006**, *2*, 636–639.
- (74) Sun, Y.; Xia, Y. Shape-controlled synthesis of gold and silver nanoparticles. *Science* **2002**, *298*, 2176–2179.

- (75) Camargo, P. H.; Au, L.; Rycenga, M.; Li, W.; Xia, Y. Measuring the SERS enhancement factors of dimers with different structures constructed from silver nanocubes. *Chem. Phys. Lett.* **2010**, *484*, 304–308.
- (76) Rycenga, M.; Camargo, P. H. C.; Li, W.; Moran, C. H.; Xia, Y. Understanding the SERS effects of single silver nanoparticles and their dimers, one at a time. *J. Phys. Chem. Lett.* **2010**, *1*, 696–703.
- (77) Chaffin, E.; O'Connor, R. T.; Barr, J.; Huang, X.; Wang, Y. Dependence of SERS enhancement on the chemical composition and structure of Ag/Au hybrid nanoparticles. *J. Chem. Phys.* **2016**, *145*, 054706.
- (78) Olea-Mejía, O.; Fernández-Mondragón, M.; Rodríguez-de la Concha, G.; Camacho-López, M. SERS-active Ag, Au and Ag–Au alloy nanoparticles obtained by laser ablation in liquids for sensing methylene blue. *Appl. Surf. Sci.* **2015**, *348*, 66–70.
- (79) Kim, K.; Kim, K. L.; Choi, J. Y.; Lee, H. B.; Shin, K. S. Surface enrichment of Ag atoms in Au/Ag alloy nanoparticles revealed by surface-enhanced Raman scattering of 2,6-dimethylphenyl isocyanide. *J. Phys. Chem. C* **2010**, *114*, 3448–3453.
- (80) Zhang, Y.; Liu, J.; Ahn, J.; Xiao, T.-H.; Li, Z.-Y.; Qin, D. Observing the Overgrowth of a Second Metal on Silver Cubic Seeds in Solution by Surface-Enhanced Raman Scattering. *ACS Nano* **2017**, *11*, 5080–5086.
- (81) Jiang, Y. X.; Li, J. F.; Wu, D. Y.; Yang, Z. L.; Ren, B.; Hu, J. W.; Chow, Y. L.; Tian, Z. Q. Characterization of surface water on Au core Pt-group metal shell nanoparticles coated electrodes by surface-enhanced Raman spectroscopy. *Chem. Commun.* **2007**, 4608–4610.
- (82) Li, J. F.; Huang, Y. F.; Ding, Y.; Yang, Z. L.; Li, S. B.; Zhou, X. S.; Fan, F. R.; Zhang, W.; Zhou, Z. Y.; Wu, D. Y.; Ren, B.; Wang, Z. L.; Tian, Z. Q. Shell-isolated nanoparticle-enhanced Raman spectroscopy. *Nature* **2010**, *464*, 392–395.
- (83) Li, J.-F.; Anema, J. R.; Wandlowski, T.; Tian, Z.-Q. Dielectric shell isolated and graphene shell isolated nanoparticle enhanced Raman spectroscopies and their applications. *Chem. Soc. Rev.* **2015**, *44*, 8399–8409.
- (84) Kudelski, A.; Wojtysiak, S. Silica-covered silver and gold nanoresonators for Raman analysis of surfaces of various materials. *J. Phys. Chem. C* **2012**, *116*, 16167–16174.
- (85) Uzayisenga, V.; Lin, X. D.; Li, L. M.; Anema, J. R.; Yang, Z. L.; Huang, Y. F.; Lin, H. X.; Li, S. B.; Li, J. F.; Tian, Z. Q. Synthesis, characterization, and 3D-FDTD simulation of Ag@SiO<sub>2</sub> nanoparticles for shell-isolated nanoparticle-enhanced Raman spectroscopy. *Langmuir* **2012**, *28*, 9140–9146.
- (86) Lin, M.; Wang, Y.; Sun, X.; Wang, W.; Chen, L. Elastic<sup>†</sup> property of mesoporous silica shell: For dynamic surface enhanced Raman scattering ability monitoring of growing noble metal nanostructures via a simplified spatially confined growth method. *ACS Appl. Mater. Interfaces* **2015**, *7*, 7516–7525.
- (87) Lee, C.; Zhang, P. Facile synthesis of gelatin-protected silver nanoparticles for SERS applications. *J. Raman Spectrosc.* **2013**, *44*, 823–826.
- (88) Bian, X.; Song, Z. L.; Qian, Y.; Gao, W.; Cheng, Z. Q.; Chen, L.; Liang, H.; Ding, D.; Nie, X. K.; Chen, Z.; Tan, W. Fabrication of graphene-isolated-Au-nanocrystal nanostructures for multimodal cell imaging and photothermal-enhanced chemotherapy. *Sci. Rep.* **2015**, *4*, 6093.
- (89) Liu, Y. M.; Hu, Y.; Zhang, J. Few-layer graphene-encapsulated metal nanoparticles for surface-enhanced Raman spectroscopy. *J. Phys. Chem. C* **2014**, *118*, 8993–8998.
- (90) Song, Z. L.; Chen, Z.; Bian, X.; Zhou, L. Y.; Ding, D.; Liang, H.; Zou, Y. X.; Wang, S. S.; Chen, L.; Yang, C.; Zhang, X. B.; Tan, W. Alkyne-functionalized superstable graphitic silver nanoparticles for Raman imaging. *J. Am. Chem. Soc.* **2014**, *136*, 13558–13561.
- (91) Yang, D.; Xia, L.; Zhao, H.; Hu, X.; Liu, Y.; Li, J.; Wan, X. Preparation and characterization of an ultrathin carbon shell coating a silver core for shell-isolated nanoparticle-enhanced Raman spectroscopy. *Chem. Commun.* **2011**, *47*, 5873–5875.
- (92) Ye, W.; Huang, H.; Yang, W.; Wang, X.; Ren, C.; Hu, Q.; Li, Y.; Ren, B. Ultrathin polydopamine film coated gold nanoparticles: a sensitive, uniform, and stable SHINERS substrate for detection of benzotriazole. *Analyst* **2017**, *142*, 3459–3467.
- (93) Zhang, Y. J.; Chen, Q. Q.; Chen, X.; Wang, A.; Tian, Z. Q.; Li, J. F. Graphene-coated Au nanoparticle-enhanced Raman spectroscopy. *J. Raman Spectrosc.* **2021**, *52*, 439–445.
- (94) Kneipp, K.; Wang, Y.; Kneipp, H.; Perelman, L. T.; Itzkan, I.; Dasari, R.; Feld, M. S. Single molecule detection using surface-enhanced Raman scattering (SERS). *Phys. Rev. Lett.* **1997**, *78*, 1667–1670.
- (95) Chen, M.; Zhang, H.; Ge, Y.; Yang, S.; Wang, P.; Fang, Y. Surface-nanostructured single silver nanowire: A new one-dimensional microscale surface-enhanced Raman scattering interface. *Langmuir* **2018**, *34*, 15160–15165.
- (96) Fang, Y.; Wei, H.; Hao, F.; Nordlander, P.; Xu, H. Remote-excitation surface-enhanced Raman scattering using propagating Ag nanowire plasmons. *Nano Lett.* **2009**, *9*, 2049–2053.
- (97) Dasgupta, A.; Singh, D.; Pavan Kumar, G. V. Dual-path remote-excitation surface enhanced Raman microscopy with plasmonic nanowire dimer. *Appl. Phys. Lett.* **2013**, *103*, 151114.
- (98) Lee, S. J.; Morrill, A. R.; Moskovits, M. Hot spots in silver nanowire bundles for surface-enhanced Raman spectroscopy. *J. Am. Chem. Soc.* **2006**, *128*, 2200–2201.
- (99) Jeong, D. H.; Zhang, Y. X.; Moskovits, M. Polarized surface enhanced Raman scattering from aligned silver nanowire rafts. *J. Phys. Chem. B* **2004**, *108*, 12724–12728.
- (100) Gunawidjaja, R.; Peleshanko, S.; Ko, H.; Tsukruk, V. V. Bimetallic nanocobs: Decorating silver nanowires with gold nanoparticles. *Adv. Mater.* **2008**, *20*, 1544–1549.
- (101) Chen, L. M.; Liu, Y. N. Ag-nanoparticle-modified single Ag nanowire for detection of melamine by surface-enhanced Raman spectroscopy. *J. Raman Spectrosc.* **2012**, *43*, 986–991.
- (102) Caires, A. J.; Vaz, R. P.; Fantini, C.; Ladeira, L. O. Highly sensitive and simple SERS substrate based on photochemically generated carbon nanotubes-gold nanorods hybrids. *J. Colloid Interface Sci.* **2015**, *455*, 78–82.
- (103) Sun, Y.; Liu, K.; Miao, J.; Wang, Z.; Tian, B.; Zhang, L.; Li, Q.; Fan, S.; Jiang, K. Highly Sensitive Surface-Enhanced Raman Scattering Substrate Made from Superaligned Carbon Nanotubes. *Nano Lett.* **2010**, *10*, 1747–1753.
- (104) Zhang, K.; Ji, J.; Fang, X.; Yan, L.; Liu, B. Carbon nanotube/gold nanoparticle composite-coated membrane as a facile plasmon-enhanced interface for sensitive SERS sensing. *Analyst* **2015**, *140* (1), 134–139.
- (105) Choo, H.; Kim, M.-K.; Staffaroni, M.; Seok, T. J.; Bokor, J.; Cabrini, S.; Schuck, P. J.; Wu, M. C.; Yablonovitch, E. Nanofocusing in a metal–insulator–metal gap plasmon waveguide with a three-dimensional linear taper. *Nat. Photonics* **2012**, *6*, 838–844.
- (106) Zhou, Z.; Zhao, Z.; Yu, Y.; Ai, B.; Möhwald, H.; Chiechi, R. C.; Yang, J. K. W.; Zhang, G. From 1D to 3D: Tunable sub-10 nm gaps in large area devices. *Adv. Mater.* **2016**, *28*, 2956–2963.
- (107) Weimer, W. A.; Dyer, M. J. Tunable surface plasmon resonance silver films. *Appl. Phys. Lett.* **2001**, *79*, 3164–3166.
- (108) Si, S. R.; Liang, W. K.; Sun, Y. H.; Huang, J.; Ma, W. L.; Liang, Z. Q.; Bao, Q. L.; Jiang, L. Facile fabrication of high-density sub-1-nm gaps from Au nanoparticle monolayers as reproducible SERS substrates. *Adv. Funct. Mater.* **2016**, *26*, 8137–8145.
- (109) Lin, Y.; Zhang, Y. J.; Yang, W. M.; Dong, J. C.; Fan, F. R.; Zhao, Y.; Zhang, H.; Bodappa, N.; Tian, X. D.; Yang, Z. L.; Stucky, G. D.; Tian, Z. Q.; Li, J. F. Size and dimension dependent surface-enhanced Raman scattering properties of well-defined Ag nanocubes. *Applied Materials Today* **2019**, *14*, 224–232.
- (110) Haynes, C. L.; Van Duyne, R. P. Nanosphere lithography: A versatile nanofabrication tool for studies of size-dependent nanoparticle optics. *J. Phys. Chem. B* **2001**, *105*, 5599–5611.
- (111) Haes, A. J.; Haynes, C. L.; Van Duyne, R. P. Nanosphere lithography: Self-assembled photonic and magnetic materials. *MRS Online Proceedings Library* **2000**, *636*, 481.

- (112) Hulteen, J. C.; Van Duyne, R. P. Nanosphere lithography: A materials general fabrication process for periodic particle array surfaces. *J. Vac. Sci. Technol. A* **1995**, *13*, 1553–1558.
- (113) Jensen, T. R.; Schatz, G. C.; Van Duyne, R. P. Nanosphere lithography: Surface plasmon resonance spectrum of a periodic array of silver nanoparticles by ultraviolet-visible extinction spectroscopy and electrodynamic modeling. *J. Phys. Chem. B* **1999**, *103*, 2394–2401.
- (114) Cinel, N. A.; Cakmakyapan, S.; Butun, S.; Ertas, G.; Ozbay, E. E-Beam lithography designed substrates for surface enhanced Raman spectroscopy. *Photonics and Nanostructures - Fundam. Appl.* **2015**, *15*, 109–115.
- (115) Kahl, M.; Voges, E.; Kostrewa, S.; Viets, C.; Hill, W. Periodically structured metallic substrates for SERS. *Sens. Actuators, B* **1998**, *51*, 285–291.
- (116) Beermann, J.; Novikov, S. M.; Leosson, K.; Bozhevolnyi, S. I. Surface enhanced Raman imaging: Periodic arrays and individual metal nanoparticles. *Opt. Express* **2009**, *17*, 12698–12705.
- (117) Yue, W.; Wang, Z.; Yang, Y.; Chen, L.; Syed, A.; Wong, K.; Wang, X. Electron-beam lithography of gold nanostructures for surface-enhanced Raman scattering. *J. Micromech. Microeng.* **2012**, *22*, 125007.
- (118) Cinel, N. A.; Cakmakyapan, S.; Ertaş, G.; Özbay, E. Concentric ring structures as efficient SERS substrates. *IEEE J. Sel. Top. Quantum Electron.* **2013**, *19*, 4601605.
- (119) Fromm, D. P.; Sundaramurthy, A.; Schuck, P. J.; Kino, G.; Moerner, W. Gap-dependent optical coupling of single “bowtie” nanoantennas resonant in the visible. *Nano Lett.* **2004**, *4*, 957–961.
- (120) Cakmakyapan, S.; Cinel, N. A.; Cakmak, A. O.; Ozbay, E. Validation of electromagnetic field enhancement in near-infrared through Sierpinski fractal nanoantennas. *Opt. Express* **2014**, *22*, 19504.
- (121) Volpe, G.; Volpe, G.; Quidant, R. Fractal plasmonics: Subdiffraction focusing and broadband spectral response by a Sierpinski nanocarpenter. *Opt. Express* **2011**, *19*, 3612–3618.
- (122) Novoselov, K. S.; Geim, A. K.; Morozov, S. V.; Jiang, D.; Zhang, Y.; Dubonos, S. V.; Grigorieva, I. V.; Firsov, A. A. Electric field effect in atomically thin carbon films. *Science* **2004**, *306*, 666–669.
- (123) Ling, X.; Xie, L.; Fang, Y.; Xu, H.; Zhang, H.; Kong, J.; Dresselhaus, M. S.; Zhang, J.; Liu, Z. Can graphene be used as a substrate for Raman enhancement? *Nano Lett.* **2010**, *10*, 553–561.
- (124) Ling, X.; Zhang, J. First-layer effect in graphene-enhanced Raman scattering. *Small* **2010**, *6*, 2020–2025.
- (125) Ling, X.; Wu, J. X.; Xie, L. M.; Zhang, J. Graphene-thickness-dependent graphene-enhanced Raman scattering. *J. Phys. Chem. C* **2013**, *117*, 2369–2376.
- (126) Seo, J.; Lee, J.; Kim, Y.; Koo, D.; Lee, G.; Park, H. Ultrasensitive plasmon-free surface-enhanced Raman spectroscopy with femtomolar detection limit from 2D van der Waals heterostructure. *Nano Lett.* **2020**, *20*, 1620–1630.
- (127) Ling, X.; Fang, W.; Lee, Y.-H.; Araujo, P. T.; Zhang, X.; Rodriguez-Nieva, J. F.; Lin, Y.; Zhang, J.; Kong, J.; Dresselhaus, M. S. Raman enhancement effect on two-dimensional layered materials: Graphene, h-BN and MoS<sub>2</sub>. *Nano Lett.* **2014**, *14*, 3033–3040.
- (128) Sun, L.; Hu, H.; Zhan, D.; Yan, J.; Liu, L.; Teguh, J. S.; Yeow, E. K.; Lee, P. S.; Shen, Z. Plasma modified MoS<sub>2</sub> nanoflakes for surface enhanced Raman scattering. *Small* **2014**, *10*, 1090–1095.
- (129) Yin, Y.; Miao, P.; Zhang, Y.; Han, J.; Zhang, X.; Gong, Y.; Gu, L.; Xu, C.; Yao, T.; Xu, P.; Wang, Y.; Song, B.; Jin, S. Significantly increased Raman enhancement on MoX<sub>2</sub> (X = S, Se) monolayers upon phase transition. *Adv. Funct. Mater.* **2017**, *27*, 1606694.
- (130) Chen, M.; Ji, B.; Dai, Z.; Du, X.; He, B.; Chen, G.; Liu, D.; Chen, S.; Lo, K. H.; Wang, S.; Zhou, B.; Pan, H. Vertically-aligned 1T/2H-MS<sub>2</sub> (M = Mo, W) nanosheets for surface-enhanced Raman scattering with long-term stability and large-scale uniformity. *Appl. Surf. Sci.* **2020**, *527*, 146769.
- (131) Song, X.; Wang, Y.; Zhao, F.; Li, Q.; Ta, H. Q.; Rummeli, M. H.; Tully, C. G.; Li, Z.; Yin, W. J.; Yang, L.; Lee, K. B.; Yang, J.; Bozkurt, I.; Liu, S.; Zhang, W.; Chhowalla, M. Plasmon-free surface-enhanced Raman spectroscopy using metallic 2D materials. *ACS Nano* **2019**, *13*, 8312–8319.
- (132) Lee, Y.; Kim, H.; Lee, J.; Yu, S. H.; Hwang, E.; Lee, C.; Ahn, J.-H.; Cho, J. H. Enhanced Raman scattering of rhodamine 6G films on two-dimensional transition metal dichalcogenides correlated to photoinduced charge transfer. *Chem. Mater.* **2016**, *28*, 180–187.
- (133) Tao, L.; Chen, K.; Chen, Z.; Cong, C.; Qiu, C.; Chen, J.; Wang, X.; Chen, H.; Yu, T.; Xie, W.; Deng, S.; Xu, J. B. 1T' transition metal telluride atomic layers for plasmon-free SERS at femtomolar levels. *J. Am. Chem. Soc.* **2018**, *140*, 8696–8704.
- (134) Naguib, M.; Kurtoglu, M.; Presser, V.; Lu, J.; Niu, J.; Heon, M.; Hultman, L.; Gogotsi, Y.; Barsoum, M. W. Two-dimensional nanocrystals produced by exfoliation of Ti<sub>3</sub>AlC<sub>2</sub>. *Adv. Mater.* **2011**, *23*, 4248–4253.
- (135) Sarycheva, A.; Makaryan, T.; Maleski, K.; Satheeshkumar, E.; Melikyan, A.; Minassian, H.; Yoshimura, M.; Gogotsi, Y. Two-dimensional titanium carbide (MXene) as surface-enhanced Raman scattering substrate. *J. Phys. Chem. C* **2017**, *121*, 19983–19988.
- (136) Soundiraraju, B.; George, B. K. Two-dimensional titanium nitride (Ti<sub>2</sub>N) MXene: synthesis, characterization, and potential application as surface-enhanced Raman scattering substrate. *ACS Nano* **2017**, *11*, 8892–8900.
- (137) Chen, M.; Liu, D.; Du, X.; Lo, K. H.; Wang, S.; Zhou, B.; Pan, H. 2D materials: Excellent substrates for surface-enhanced Raman scattering (SERS) in chemical sensing and biosensing. *Trends Analyt. Chem.* **2020**, *130*, 115983.
- (138) Valeš, V.; Kovaricek, P.; Fridrichova, M.; Ji, X.; Ling, X.; Kong, J.; Dresselhaus, M. S.; Kalbac, M. Enhanced Raman scattering on functionalized graphene substrates. *2D Mater.* **2017**, *4*, 025087.
- (139) Huh, S.; Park, J.; Kim, Y. S.; Kim, K. S.; Hong, B. H.; Nam, J. M. UV/ozone-oxidized large-scale graphene platform with large chemical enhancement in surface-enhanced Raman scattering. *ACS Nano* **2011**, *5*, 9799–9806.
- (140) Tan, Y.; Ma, L.; Gao, Z.; Chen, M.; Chen, F. Two-dimensional heterostructure as a platform for surface-enhanced Raman scattering. *Nano Lett.* **2017**, *17*, 2621–2626.
- (141) Lu, J.; Lu, J. H.; Liu, H.; Liu, B.; Gong, L.; Tok, E. S.; Loh, K. P.; Sow, C. H. Microlandscaping of Au nanoparticles on few-layer MoS<sub>2</sub> films for chemical sensing. *Small* **2015**, *11*, 1792–1800.
- (142) Wang, P.; Liang, O.; Zhang, W.; Schroeder, T.; Xie, Y. H. Ultra-sensitive graphene-plasmonic hybrid platform for label-free detection. *Adv. Mater.* **2013**, *25*, 4918–4924.
- (143) Liu, X.; Wang, J.; Wu, Y.; Fan, T.; Xu, Y.; Tang, L.; Ying, Y. Compact shielding of graphene monolayer leads to extraordinary SERS-active substrate with large-area uniformity and long-term stability. *Sci. Rep.* **2015**, *5*, 17167.
- (144) Shaik, U. P.; Hamad, S.; Ahamad Mohiddin, Md.; Soma, V. R.; Ghanashyam Krishna, M. Morphologically manipulated Ag/ZnO nanostructures as surface enhanced Raman scattering probes for explosives detection. *J. Appl. Phys.* **2016**, *119*, 093103.
- (145) Zhang, X.; Xiao, X.; Dai, Z.; Wu, W.; Zhang, X.; Fu, L.; Jiang, C. Ultrasensitive SERS performance in 3D “sunflower-like” nanoarrays decorated with Ag nanoparticles. *Nanoscale* **2017**, *9*, 3114–3120.
- (146) Huang, Z. L.; Meng, G. W.; Huang, Q.; Chen, B.; Zhu, C. H.; Zhang, Z. Large-area Ag nanorod array substrates for SERS: AAO template-assisted fabrication, functionalization, and application in detection PCBs. *J. Raman Spectrosc.* **2013**, *44*, 240–246.
- (147) Park, S. G.; Mun, C.; Lee, M.; Jeon, T. Y.; Shim, H. S.; Lee, Y. J.; Kwon, J. D.; Kim, C. S.; Kim, D. H. 3D hybrid plasmonic nanomaterials for highly efficient optical absorbers and sensors. *Adv. Mater.* **2015**, *27*, 4290–4295.
- (148) Leem, J.; Wang, M. C.; Kang, P.; Nam, S. Mechanically self-assembled, three-dimensional graphene-gold hybrid nanostructures for advanced nanoplasmonic sensors. *Nano Lett.* **2015**, *15*, 7684–7690.
- (149) Urban, A. S.; Shen, X.; Wang, Y.; Large, N.; Wang, H.; Knight, M. W.; Nordlander, P.; Chen, H.; Halas, N. J. Three-dimensional plasmonic nanoclusters. *Nano Lett.* **2013**, *13*, 4399–4403.

- (150) Chen, J.; Martensson, T.; Dick, K. A.; Deppert, K.; Xu, H. Q.; Samuelson, L.; Xu, H. Surface-enhanced Raman scattering of rhodamine 6G on nanowire arrays decorated with gold nanoparticles. *Nanotechnology* **2008**, *19*, 275712.
- (151) Cheung, C. L.; Nikolić, R. J.; Reinhardt, C. E.; Wang, T. F. Fabrication of nanopillars by nanosphere lithography. *Nanotechnology* **2006**, *17*, 1339–1343.
- (152) Wang, Y.; Becker, M.; Wang, L.; Liu, J.; Scholz, R.; Peng, J.; Gösele, U.; Christiansen, S.; Kim, D. H.; Steinhart, M. Nanostructured gold films for SERS by block copolymer-templated galvanic displacement reactions. *Nano Lett.* **2009**, *9*, 2384–2389.
- (153) Shi, G.; Wang, M.; Zhu, Y.; Yan, X.; Pan, S.; Zhang, A. Nanoflower-like Ag/AAO SERS platform with quasi-photon crystal nanostructure for efficient detection of goat serum. *Curr. Appl. Phys.* **2019**, *19*, 1276–1285.
- (154) Chung, A. J.; Huh, Y. S.; Erickson, D. Large area flexible SERS active substrates using engineered nanostructures. *Nanoscale* **2011**, *3*, 2903–2908.
- (155) Yakimchuk, D. V.; Prigodich, U. V.; Demyanov, S. E.; Ustarroz, J.; Terryn, H.; Baert, K.; Khubezhov, S. A.; Tishkevich, D. I.; Trukhanov, A. V.; Sivakov, V.; Kaniukov, E. Y. Growth mechanism study of silver nanostructures in a limited volume. *Mater. Chem. Phys.* **2022**, *283*, 126016.
- (156) Guan, Y.; Wang, Z.; Gu, P.; Wang, Y.; Zhang, W.; Zhang, G. An in situ SERS study of plasmonic nanochemistry based on bifunctional “hedgehog-like” arrays. *Nanoscale* **2019**, *11*, 9422–9428.
- (157) Chen, B.; Meng, G.; Huang, Q.; Huang, Z.; Xu, Q.; Zhu, C.; Qian, Y.; Ding, Y. Green synthesis of large-scale highly ordered core@shell nanoporous Au@Ag nanorod arrays as sensitive and reproducible 3D SERS substrates. *ACS Appl. Mater. Interfaces* **2014**, *6*, 15667–15675.
- (158) Fu, Q.; Zhan, Z.; Dou, J.; Zheng, X.; Xu, R.; Wu, M.; Lei, Y. Highly reproducible and sensitive SERS substrates with Ag inter-nanoparticle gaps of 5 nm fabricated by ultrathin aluminum mask technique. *ACS Appl. Mater. Interfaces* **2015**, *7*, 13322–13328.
- (159) Tian, C.; Li, J.; Ma, C.; Wang, P.; Sun, X.; Fang, J. An ordered mesoporous Ag superstructure synthesized via a template strategy for surface-enhanced Raman spectroscopy. *Nanoscale* **2015**, *7*, 12318–12324.
- (160) Ding, Q.; Kang, Z.; He, X.; Wang, M.; Lin, M.; Lin, H.; Yang, D.-P. Eggshell membrane-templated gold nanoparticles as a flexible SERS substrate for detection of thiabendazole. *Microchim. Acta* **2019**, *186*, 453.
- (161) Jin, H. M.; Kim, J. Y.; Heo, M.; Jeong, S. J.; Kim, B. H.; Cha, S. K.; Han, K. H.; Kim, J. H.; Yang, G. G.; Shin, J.; Kim, S. O. Ultralarge area sub-10 nm plasmonic nanogap array by block copolymer self-assembly for reliable high-sensitivity SERS. *ACS Appl. Mater. Interfaces* **2018**, *10*, 44660–44667.
- (162) Huo, D.; Chen, B.; Meng, G.; Huang, Z.; Li, M.; Lei, Y. Ag-nanoparticles@bacterial nanocellulose as a 3D flexible and robust surface-enhanced Raman scattering substrate. *ACS Appl. Mater. Interfaces* **2020**, *12*, 50713–50720.
- (163) Zhang, J.; Zhang, X. L.; Chen, S. M.; Gong, T. C.; Zhu, Y. Surface-enhanced Raman scattering properties of multi-walled carbon nanotubes arrays-Ag nanoparticles. *Carbon* **2016**, *100*, 395–407.
- (164) Ling, Y. H.; Zhuo, Y. Q.; Huang, L.; Mao, D. L. Using Ag-embedded TiO<sub>2</sub> nanotubes array as recyclable SERS substrate. *Appl. Surf. Sci.* **2016**, *388*, 169–173.
- (165) Quan, Y.; Yao, J.; Yang, S.; Chen, L.; Liu, Y.; Lang, J.; Zeng, H.; Yang, J.; Gao, M. Detect, remove and re-use: Sensing and degradation pesticides via 3D tilted ZMRs/Ag arrays. *J. Hazard. Mater.* **2020**, *391*, 122222.
- (166) Ossig, R.; Kolomijeca, A.; Kwon, Y.-H.; Hubenthal, F.; Kronfeldt, H.-D. SERS signal response and SERS/SERDS spectra of fluoranthene in water on naturally grown Ag nanoparticle ensembles. *J. Raman Spectrosc.* **2013**, *44*, 717–722.
- (167) Mao, P.; Liu, C.; Favraud, G.; Chen, Q.; Han, M.; Fratolocchi, A.; Zhang, S. Broadband single molecule SERS detection designed by warped optical spaces. *Nat. Commun.* **2018**, *9*, 5428.
- (168) Gandra, N.; Abbas, A.; Tian, L.; Singamaneni, S. Plasmonic planet-satellite analogues: hierarchical self-assembly of gold nanostructures. *Nano Lett.* **2012**, *12*, 2645–2651.
- (169) Mueller, N. S.; Pfitzner, E.; Okamura, Y.; Gordeev, G.; Kusch, P.; Lange, H.; Heberle, J.; Schulz, F.; Reich, S. Surface-enhanced Raman scattering and surface-enhanced infrared absorption by plasmon polaritons in three-dimensional nanoparticle supercrystals. *ACS Nano* **2021**, *15*, 5523–5533.
- (170) Hu, Y.; Liao, J.; Wang, D.; Li, G. Fabrication of gold nanoparticle-embedded metal-organic framework for highly sensitive surface-enhanced Raman scattering detection. *Anal. Chem.* **2014**, *86*, 3955–3963.
- (171) Lu, S.; You, T.; Gao, Y.; Yang, N.; Zhang, C.; Yin, P. Rapid fabrication of three-dimensional flower-like gold microstructures on flexible substrate for SERS applications. *Spectrochim. Acta A Mol. Biomol. Spectrosc.* **2019**, *212*, 371–379.
- (172) Oh, Y.-J.; Kang, M.; Park, M.; Jeong, K.-H. Engineering hot spots on plasmonic nanopillar arrays for SERS: A review. *BioChip J.* **2016**, *10*, 297–309.
- (173) Akinoglu, G. E.; Hutchison, J. A. Perspective—Quasi-Babinet complementary plasmonic templates: A platform to perform spectroelectrochemistry. *ECS J. Solid State Sci. Technol.* **2021**, *10*, 035005.
- (174) Men, D.; Wu, Y.; Wang, C.; Xiang, J.; Yang, G.; Wan, C.; Zhang, H. Wafer-scale hierarchical nanopillar arrays based on Au masks and reactive ion etching for effective 3D SERS substrate. *Materials* **2018**, *11*, 239.
- (175) Xu, X.; Yang, Q.; Wattanatorn, N.; Zhao, C.; Chiang, N.; Jonas, S. J.; Weiss, P. S. Multiple-patterning nanosphere lithography for fabricating periodic three-dimensional hierarchical nanostructures. *ACS Nano* **2017**, *11*, 10384–10391.
- (176) Baek, S. H.; Lee, S.; Bae, J.-H.; Hong, C.-W.; Park, M.-J.; Park, H.; Baek, M.-C.; Nam, S.-W. Nanopillar and nanohole fabrication via mixed lithography. *Mater. Res. Express* **2020**, *7*, 035008.
- (177) Doll, P. W.; Al-Ahmad, A.; Bacher, A.; Muslija, A.; Thelen, R.; Hahn, L.; Ahrens, R.; Spindler, B.; Guber, A. E. Fabrication of silicon nanopillar arrays by electron beam lithography and reactive ion etching for advanced bacterial adhesion studies. *Mater. Res. Express* **2019**, *6*, 065402.
- (178) Li, W.-D.; Ding, F.; Hu, J.; Chou, S. Y. Three-dimensional cavity nanoantenna coupled plasmonic nanodots for ultrahigh and uniform surface-enhanced Raman scattering over large area. *Opt. Express* **2011**, *19*, 3925–3936.
- (179) Hu, M.; Ou, F. S.; Wu, W.; Naumov, I.; Li, X.; Bratkovsky, A. M.; Williams, R. S.; Li, Z. Gold nanofingers for molecule trapping and detection. *J. Am. Chem. Soc.* **2010**, *132*, 12820–12822.
- (180) Chattopadhyay, S.; Lo, H.-C.; Hsu, C.-H.; Chen, L.-C.; Chen, K.-H. Surface-enhanced Raman spectroscopy using self-assembled silver nanoparticles on silicon nanotips. *Chem. Mater.* **2005**, *17*, 553–559.
- (181) Tang, J.; Ou, F. S.; Kuo, H. P.; Hu, M.; Stickle, W. F.; Li, Z.; Williams, R. S. Silver-coated Si nanograss as highly sensitive surface-enhanced Raman spectroscopy substrates. *Appl. Phys. A: Mater. Sci. Process.* **2009**, *96*, 793–797.
- (182) Akinoglu, G. E.; Mir, S. H.; Gatensby, R.; Rydzek, G.; Mokarian-Tabari, P. Block copolymer derived vertically coupled plasmonic arrays for surface-enhanced Raman spectroscopy. *ACS Appl. Mater. Interfaces* **2020**, *12*, 23410–23416.
- (183) Li, T.; Wu, K.; Rindzevicius, T.; Wang, Z.; Schulte, L.; Schmidt, M. S.; Boisen, A.; Ndoni, S. Wafer-scale nanopillars derived from block copolymer lithography for surface-enhanced Raman spectroscopy. *ACS Appl. Mater. Interfaces* **2016**, *8*, 15668–15675.
- (184) Lafuente, M.; Berenschot, E. J. W.; Tiggelaar, R. M.; Rodrigo, S. G.; Mallada, R.; Tas, N. R.; Pina, M. P. Attomolar SERS detection of organophosphorous pesticides using silver mirror-like micro-pyramids as active substrate. *Microchim. Acta* **2020**, *187*, 247.
- (185) Cinel, N. A.; Butun, S.; Ertas, G.; Ozbay, E. ‘Fairly Chimney’-shaped tandem metamaterials as double resonance SERS substrates. *Small* **2013**, *9*, 531–537.

- (186) Schmidt, M. S.; Hubner, J.; Boisen, A. Large area fabrication of leaning silicon nanopillars for surface enhanced Raman spectroscopy. *Adv. Mater.* **2012**, *24*, OP11–OP18.
- (187) Cummins, C.; Lundy, R.; Walsh, J. J.; Ponsinet, V.; Fleury, G.; Morris, M. A. Enabling future nanomanufacturing through block copolymer self-assembly: A review. *Nano Today* **2020**, *35*, 100936.
- (188) Lee, N.; Kim, R.; Kim, J. Y.; Ko, J. B.; Park, S.-H. K.; Kim, S. O.; Brongersma, M. L.; Shin, J. Self-assembled nano-lotus pod metasurface for light trapping. *ACS Photonics* **2021**, *8*, 1616–1622.
- (189) Kim, J. Y.; Kim, H.; Kim, B. H.; Chang, T.; Lim, J.; Jin, H. M.; Mun, J. H.; Choi, Y. J.; Chung, K.; Shin, J.; Fan, S.; Kim, S. O. Highly tunable refractive index visible-light metasurface from block copolymer self-assembly. *Nat. Commun.* **2016**, *7*, 12911.
- (190) Cummins, C.; Ghoshal, T.; Holmes, J. D.; Morris, M. A. Strategies for inorganic incorporation using neat block copolymer thin films for etch mask function and nanotechnological application. *Adv. Mater.* **2016**, *28*, 5586–5618.
- (191) Wu, K.; Li, T.; Schmidt, M. S.; Rindzevicius, T.; Boisen, A.; Ndoni, S. Gold nanoparticles sliding on recyclable nanohoodoos—Engineered for surface-enhanced Raman spectroscopy. *Adv. Funct. Mater.* **2018**, *28*, 1704818.
- (192) Ma, B.; Li, P.; Yang, L.; Liu, J. Based on time and spatial-resolved SERS mapping strategies for detection of pesticides. *Talanta* **2015**, *141*, 1–7.
- (193) Qian, K.; Yang, L.; Li, Z.; Liu, J. A new-type dynamic SERS method for ultrasensitive detection. *J. Raman Spectrosc.* **2013**, *44*, 21–28.
- (194) Fujita, K.; Ishitobi, S.; Hamada, K.; Smith, N. I.; Taguchi, A.; Inouye, Y.; Kawata, S. Time-resolved observation of surface-enhanced Raman scattering from gold nanoparticles during transport through a living cell. *J. Biomed. Opt.* **2009**, *14*, 024038.
- (195) Xu, Z. Z.; Liang, Z. B.; Guo, W. H.; Zou, R. Q. In situ/operando vibrational spectroscopy for the investigation of advanced nanostructured electrocatalysts. *Coord. Chem. Rev.* **2021**, *436*, 213824.
- (196) Wen, B.-Y.; Chen, Q.-Q.; Radjenovic, P. M.; Dong, J.-C.; Tian, Z.-Q.; Li, J.-F. In situ surface-enhanced Raman spectroscopy characterization of electrocatalysis with different nanostructures. *Annu. Rev. Phys. Chem.* **2021**, *72*, 331–351.
- (197) An, H.; Wu, L.; Mandemaker, L. D. B.; Yang, S.; Ruiters, J.; Wijten, J. H. J.; Janssens, J. C. L.; Hartman, T.; Stam, W.; Weckhuysen, B. M. Sub-second time-resolved surface-enhanced Raman spectroscopy reveals dynamic CO intermediates during electrochemical CO<sub>2</sub> reduction on copper. *Angew. Chem., Int. Ed.* **2021**, *60*, 16576–16584.
- (198) Dong, J.-C.; Zhang, X.-G.; Briega-Martos, V.; Jin, X.; Yang, J.; Chen, S.; Yang, Z.-L.; Wu, D.-Y.; Feliu, J. M.; Williams, C. T.; Tian, Z.-Q.; Li, J.-F. In situ Raman spectroscopic evidence for oxygen reduction reaction intermediates at platinum single-crystal surfaces. *Nat. Energy* **2019**, *4*, 60–67.
- (199) Chen, J.; Liu, G.; Zhu, Y.-z.; Su, M.; Yin, P.; Wu, X.-j.; Lu, Q.; Tan, C.; Zhao, M.; Liu, Z.; Yang, W.; Li, H.; Nam, G.-H.; Zhang, L.; Chen, Z.; Huang, X.; Radjenovic, P. M.; Huang, W.; Tian, Z.-q.; Li, J.-f.; Zhang, H. Ag@MoS<sub>2</sub> core-shell heterostructure as SERS platform to reveal the hydrogen evolution active sites of single-layer MoS<sub>2</sub>. *J. Am. Chem. Soc.* **2020**, *142*, 7161–7167.
- (200) Radjenovic, P. M.; Hardwick, L. J. Time-resolved SERS study of the oxygen reduction reaction in ionic liquid electrolytes for non-aqueous lithium–oxygen cells. *Faraday Discuss.* **2018**, *206*, 379–392.
- (201) Kim, K. H.; Kim, J. G.; Nozawa, S.; Sato, T.; Oang, K. Y.; Kim, T. W.; Ki, H.; Jo, J.; Park, S.; Song, C.; Sato, T.; Ogawa, K.; Togashi, T.; Tono, K.; Yabashi, M.; Ishikawa, T.; Kim, J.; Ryoo, R.; Kim, J.; Ihee, H.; Adachi, S. Direct observation of bond formation in solution with femtosecond X-ray scattering. *Nature* **2015**, *518*, 385–389.
- (202) Pavlovic, Z.; Ranjan, C.; Gao, Q.; van Gastel, M.; Schlögl, R. Probing the Structure of a Water-Oxidizing Anodic Iridium Oxide Catalyst using Raman Spectroscopy. *ACS Catal.* **2016**, *6*, 8098–8105.
- (203) Mandal, L.; Yang, K. R.; Motapothula, M. R.; Ren, D.; Lobaccaro, P.; Patra, A.; Sherburne, M.; Batista, V. S.; Yeo, B. S.; Ager, J. W.; Martin, J.; Venkatesan, T. Investigating the role of copper oxide in electrochemical CO<sub>2</sub> reduction in real time. *ACS Appl. Mater. Interfaces* **2018**, *10*, 8574–8584.
- (204) Dietze, D. R.; Mathies, R. A. Femtosecond stimulated Raman spectroscopy. *ChemPhysChem* **2016**, *17*, 1224–1251.
- (205) Ruhman, S.; Joly, A. G.; Nelson, K. A. Time-resolved observations of coherent molecular vibrational motion and the general occurrence of impulsive stimulated scattering. *J. Chem. Phys.* **1987**, *86*, 6563–6565.
- (206) Yoshizawa, M.; Hattori, Y.; Kobayashi, T. Femtosecond time-resolved resonance Raman gain spectroscopy in polydiacetylene. *Phys. Rev. B* **1994**, *49*, 13259–13262.
- (207) Bell, S. E. J. Tutorial review. Time-resolved resonance Raman spectroscopy. *Analyst* **1996**, *121*, 107R–120R.
- (208) Silva, W. R.; Graefe, C. T.; Frontiera, R. R. Toward label-free super-resolution microscopy. *ACS Photonics* **2016**, *3*, 79–86.
- (209) Pellatz, N.; Roy, S.; Lee, J. W.; Schäd, J. L.; Kandel, H.; Arndt, N.; Eom, C. B.; Kemper, A. F.; Reznik, D. Relaxation timescales and electron-phonon coupling in optically pumped YBa<sub>2</sub>Cu<sub>3</sub>O<sub>6+x</sub> revealed by time-resolved Raman scattering. *Phys. Rev. B* **2021**, *104*, L180505.
- (210) Zhu, J.; Bernhardt, R.; Cui, W.; German, R.; Wagner, J.; Senkovskiy, B. V.; Grüneis, A.; Pichler, T.; Li, Y.; Li, X.; Wu, K.; Liu, R.; Zhu, X.; Van Loosdrecht, P. H. M.; Shi, L. Unraveling the excitonic transition and associated dynamics in confined long linear carbon chains with time-resolved resonance Raman scattering. *Laser Photonics Rev.* **2021**, *15*, 2100259.
- (211) Ellis, S. R.; Hoffman, D. P.; Park, M.; Mathies, R. A. Difference bands in time-resolved femtosecond stimulated Raman spectra of photoexcited intermolecular electron transfer from chloronaphthalene to tetracyanoethylene. *J. Phys. Chem. A* **2018**, *122*, 3594–3605.
- (212) Coppola, F.; Cimino, P.; Raucci, U.; Chiariello, M. G.; Petrone, A.; Rega, N. Exploring the Franck–Condon region of a photoexcited charge transfer complex in solution to interpret femtosecond stimulated Raman spectroscopy: excited state electronic structure methods to unveil non-radiative pathways. *Chem. Sci.* **2021**, *12*, 8058–8072.
- (213) Fang, C.; Frontiera, R. R.; Tran, R.; Mathies, R. A. Mapping GFP structure evolution during proton transfer with femtosecond Raman spectroscopy. *Nature* **2009**, *462*, 200–204.
- (214) Kumar, P.; Kuramochi, H.; Takeuchi, S.; Tahara, T. Time-domain observation of surface-enhanced coherent Raman scattering with 10<sup>5</sup>–10<sup>6</sup> enhancement. *J. Phys. Chem. Lett.* **2020**, *11*, 6305–6311.
- (215) Raanan, D.; Ren, L.; Oron, D.; Silberberg, Y. Impulsive Raman spectroscopy via precision measurement of frequency shift with low energy excitation. *Opt. Lett.* **2018**, *43*, 470–473.
- (216) Batignani, G.; Sansone, C.; Ferrante, C.; Fumero, G.; Mukamel, S.; Scopigno, T. Excited-state energy surfaces in molecules revealed by impulsive stimulated Raman excitation profiles. *J. Phys. Chem. Lett.* **2021**, *12*, 9239–9247.
- (217) Bian, K.; Gerber, C.; Heinrich, A. J.; Müller, D. J.; Scheuring, S.; Jiang, Y. Scanning probe microscopy. *Nat. Rev. Methods Primers* **2021**, *1*, 36.
- (218) Wessel, J. Surface-enhanced optical microscopy. *Journal of the Optical Society of America B* **1985**, *2*, 1538–1541.
- (219) Anderson, M. S. Locally enhanced Raman spectroscopy with an atomic force microscope. *Appl. Phys. Lett.* **2000**, *76*, 3130–3132.
- (220) Hayazawa, N.; Inouye, Y.; Sekkat, Z.; Kawata, S. Metallized tip amplification of near-field Raman scattering. *Opt. Commun.* **2000**, *183*, 333–336.
- (221) Hartschuh, A.; Sanchez, E. J.; Xie, X. S.; Novotny, L. High-resolution near-field Raman microscopy of single-walled carbon nanotubes. *Phys. Rev. Lett.* **2003**, *90*, 095503.
- (222) Poliani, E.; Wagner, M. R.; Vierck, A.; Herziger, F.; Nenstiel, C.; Gannott, F.; Schweiger, M.; Fritze, S.; Dadgar, A.; Zaumseil, J.; Krost, A.; Hoffmann, A.; Maultzsch, J. Breakdown of far-field Raman selection rules by light-plasmon coupling demonstrated by tip-enhanced Raman scattering. *J. Phys. Chem. Lett.* **2017**, *8*, 5462–5471.
- (223) Gramotnev, D. K.; Bozhevolnyi, S. I. Plasmonics beyond the diffraction limit. *Nat. Photonics* **2010**, *4*, 83–91.

- (224) Keilmann, F. Surface-polariton propagation for scanning near-field optical microscopy application. *J. Microsc.* **1999**, *194*, 567–570.
- (225) Stockman, M. I. Nanofocusing of optical energy in tapered plasmonic waveguides. *Phys. Rev. Lett.* **2004**, *93*, 137404.
- (226) Ropers, C.; Neacsu, C. C.; Elsaesser, T.; Albrecht, M.; Raschke, M. B.; Lienau, C. Grating-coupling of surface plasmons onto metallic tips: A nanoconfined light source. *Nano Lett.* **2007**, *7*, 2784–2788.
- (227) Pozzi, E. A.; Sonntag, M. D.; Jiang, N.; Chiang, N.; Seideman, T.; Hersam, M. C.; Van Duyne, R. P. Ultrahigh vacuum tip-enhanced Raman spectroscopy with picosecond excitation. *J. Phys. Chem. Lett.* **2014**, *5*, 2657–2661.
- (228) Ichimura, T.; Hayazawa, N.; Hashimoto, M.; Inouye, Y.; Kawata, S. Tip-enhanced coherent anti-Stokes Raman scattering for vibrational nanoimaging. *Phys. Rev. Lett.* **2004**, *92*, 220801.
- (229) Klingsporn, J. M.; Sonntag, M. D.; Seideman, T.; Van Duyne, R. P. Tip-enhanced Raman spectroscopy with picosecond pulses. *J. Phys. Chem. Lett.* **2014**, *5*, 106–110.
- (230) Wickramasinghe, H. K.; Chaigneau, M.; Yasukuni, R.; Picardi, G.; Ossikovski, R. Billion-fold increase in tip-enhanced Raman signal. *ACS Nano* **2014**, *8*, 3421–3426.
- (231) Cocker, T. L.; Peller, D.; Yu, P.; Repp, J.; Huber, R. Tracking the ultrafast motion of a single molecule by femtosecond orbital imaging. *Nature* **2016**, *539*, 263–267.
- (232) Müller, M.; Kravtsov, V.; Paarmann, A.; Raschke, M. B.; Ernstorfer, R. Nanofocused plasmon-driven sub-10 fs electron point source. *ACS Photonics* **2016**, *3*, 611–619.
- (233) Berweger, S.; Atkin, J. M.; Xu, X. G.; Olmon, R. L.; Raschke, M. B. Femtosecond nanofocusing with full optical waveform control. *Nano Lett.* **2011**, *11*, 4309–4313.